Source of Image Contrast in STM Images of Functionalized Alkanes on Graphite: A Systematic Functional Group Approach

Christopher L. Claypool, Francesco Faglioni, William A. Goddard III, Harry B. Gray, Nathan S. Lewis,* and R. A. Marcus

Division of Chemistry and Chemical Engineering, California Institute of Technology, Pasadena, California 91125

Received: January 7, 1997; In Final Form: April 16, 1997[⊗]

A series of functionalized alkanes and/or alkyl alcohols have been prepared and imaged by scanning tunneling microscopy (STM) methods on graphite surfaces. The stability of these ordered overlayers has facilitated reproducible collection of STM images at room temperature with submolecular resolution, in most cases allowing identification of individual hydrogen atoms in the alkane chains, but in all cases allowing identification of molecular length features and other aspects of the image that can be unequivocally related to the presence of functional groups in the various molecules of concern. Functional groups imaged in this study include halides (X = F, Cl, Br, I), amines, alcohols, nitriles, alkenes, alkynes, ethers, thioethers, and disulfides. Except for −Cl and −OH, all of the other functional groups could be distinguished from each other and from −Cl or −OH through an analysis of their STM metrics and image contrast behavior. The dominance of molecular topography in producing the STM images of alkanes and alkanols was established experimentally and also was consistent with quantum chemistry calculations. Unlike the contrast of the methylene regions of the alkyl chains, the STM contrast produced by the various functional groups was not dominated by topographic effects, indicating that variations in local electronic coupling were important in producing the observed STM images of these regions of the molecules. For molecules in which electronic effects overwhelmed topographic effects in determining the image contrast, a simple model is presented to explain the variation in the electronic coupling component that produces the contrast between the various functional groups observed in the STM images. Additionally, the bias dependence of these STM images has been investigated and the contrast vs bias behavior is related to factors involving electron transfer and hole transfer that have been identified as potentially being important in dominating the electronic coupling in molecular electron transfer processes.

I. Introduction

Scanning tunneling microscopy (STM) images of molecules, obtained at the resolution of individual atoms and/or functional groups, has potential for providing spatial information on electronic coupling matrix elements that are important in a variety of heterogeneous and homogeneous electron transfer processes. Although the scanning tunneling microscope[1] (STM) has been used to investigate a rapidly growing list of organic materials at surfaces and interfaces,[2] the mechanisms of electron transport through insulating organic materials are still under debate. It is thus of great theoretical and experimental interest to understand, in a systematic fashion, the factors that control the spatial image contrast in a molecular-resolution STM image.

A significant experimental barrier to advancing this subject is the lack of a controlled method of sample preparation that allows the collection of reproducible STM images that can be unequivocally assigned to the molecule of interest. At room temperature, isolated molecules are generally mobile on surfaces, and such mobility during a lateral scan with the STM tip is thought to prevent collection of reproducible STM images. In cases where individual, isolated STM images assignable to molecular features have been obtained,[3] there is a question as to whether the image actually corresponded to a region of the surface where the molecule of interest resided or whether it corresponded to a surface defect and/or tip-related imaging artifact.[4] In some cases, molecules apparently migrate to step edge sites and must be located by sorting through a large number of images that do not display the molecule of interest.[5] In other cases, defects have been shown to produce STM images that resemble biomolecules or other possible molecular species.[6a] Approaches to obviate this problem include preparation of molecular corrals[6b] in which molecules might be immobilized or the development of strategies to attach molecules covalently in a reproducible, defined fashion to smooth, STM-compatible substrates.

Another approach to circumvent this problem is to study surface/molecular overlayer combinations that spontaneously yield ordered domains of well-defined molecular monolayers. In this fashion, the same molecular structure can be reliably prepared, and observed experimentally, over a variety of experimental trials. In such systems, the STM data can be assigned with confidence to the molecule of concern. Systematic variation of the molecular size can then be used to lend confidence to the association between the object in the image and the molecule of interest; additionally, systematic variation in the identity of individual functional groups can be used to establish a relative contrast scale for probing the variation in tunneling current between sections of a molecule and/or between various types of molecules. We have adopted this strategy in this study, which was designed to elucidate several aspects of STM image contrast and to relate these features to factors thought to control electron transfer matrix elements in intramolecular and intermolecular donor/acceptor charge transfer reactions.

The basis for our work is the demonstration that long chain alkanes and alcohols adsorb from nonpolar solutions to form single, close-packed monolayers on graphite. This process has been investigated through measurement of adsorption isotherms,

[⊗] Abstract published in *Advance ACS Abstracts,* June 15, 1997.

S1089-5647(97)00179-X CCC: $14.00

enthalpies of adsorption, and adsorbed surface mass measurements.[7−10] Only a single monomolecular layer of alkanes absorbs onto highly ordered pyrolytic graphite surfaces at room temperature, and the measured heat of adsorption increases uniformly with the chain length (∼0.94 kJ/mol for each methylene unit), reaching 209 kJ/mol for dotriacontane ($C_{32}H_{66}$).[10,11] There has been some debate about whether the alkane adsorption is driven by adsorbate−substrate interactions or by lateral intermolecular interactions, but recent evidence tends to point toward the latter.[12,13] These reproducibly prepared, ordered overlayers have proven to be very amenable to study with the STM. Since the first report of imaging an alkane monolayer on graphite with a scanning tunneling microscope,[14] several reports have described images of functionalized alkanes, including alcohols,[12,15−17,19,20] carboxylic acids,[12] dialkyl-substituted benzenes,[12,18] disulfides,[19] thiols,[20] amines,[20b] and halides.[20] X-ray diffraction studies of alkane and alkanol monolayers on graphite confirm that the STM images of these organic molecules have revealed the actual arrangements of the molecules adsorbed on graphite.[21]

Unlike several other systems in the literature we have tried to reproduce, we have found that monolayers of these simple alkanes and alkanols on graphite yield highly reproducible STM images. On the basis of the reproducibility of this system and its simplicity, we have chosen this class of organic molecules to study the mechanisms underlying STM image contrast. Toward this end, a series of functionalized alkanes and/or alkyl alcohols have been prepared and imaged on graphite surfaces. We have stored over 500 images and have observed reproducible behavior during over 100 imaging sessions with almost 20 different molecules in this system. The stability of these ordered overlayers has facilitated collection of STM images at room temperature with submolecular resolution, in most cases allowing identification of individual hydrogen atoms in the alkane chains, but in all cases allowing identification of molecular length features and other aspects of the image that can be unequivocally related to the presence of functional groups in the various molecules of concern. This combination of reproducibility and submolecular resolution has allowed us to establish a contrast scale of the tunneling current for individual functional groups relative to the tunneling current over methylene groups in an alkane chain, and to relate these relative contrast features to matrix elements used to compute electronic coupling terms in electron transfer reactions. Functional groups investigated in this study include halides (X = F, Cl, Br, I), amines, alcohols, nitriles, alkenes, alkynes, ethers, thioethers, and disulfides. Additionally, we have investigated the bias dependence of these images to probe issues related to electron transfer vs hole transfer that have been identified as potentially being important in dominating the electronic coupling in molecular electron transfer processes.

II. Experimental Section

Samples were prepared by placing a 6 μL droplet of a solution of the organic compound (typically 1−10 mg/mL) in phenyloctane (except for decanol, which was used neat) onto a freshly cleaved, highly oriented pyrolytic graphite surface (HOPG, Union Carbide). A mechanically prepared Pt/Ir tip was then immersed into the liquid droplet and the imaging (Nanoscope III, Digital Instruments, Santa Barbara, CA) was performed at the liquid/graphite interface. All of the images presented were obtained at constant current in the variable height mode. Bright portions of the images displayed herein correspond to points at which the tip retracted away from the surface in order to maintain a constant current. Nearly every prepared sample yielded evidence of the adsorbed monolayer in the STM image; however, several different tips were sometimes necessary to achieve high resolution images.

The lattice spacing of graphite (2.46 Å) was used as the calibration standard for the *x* and *y* piezo dimensions. The height of a step edge on a graphite surface was determined to be 3.4 Å using the manufacturer's specifications for the *z*-piezoelectric coefficient of the ceramic. Since the separation between graphite layers is 3.35 Å, the manufacturer's specification for the *z*-piezo dimension was used in computing all *z*-corrugation values reported in this work. Metrics were determined using Nanoscope III software, and the apparent heights of heteroatoms and groups are reported with respect to the average height of the image over the methylene portion of the adsorbed molecule. Errors in the distances quoted in this article include our estimates of the measurement errors associated with determining the metrics from the images as well as the reproducibility of these metrics over various experiments. Images that displayed excessive thermal drift were not analyzed. To reduce noise, after data collection the images were filtered using Nanoscope III software. The filtering was primarily performed to enhance the visual presentation of the printed images, but the filtering was performed in such a way that it did not distort any of the primary metrics evident in the original data nor did the filtering procedure introduce any new spot patterns or new topographic features into an image.

Pentatriacontane (TCI), tetradecanol (Aldrich), dodecanol (Aldrich), decanol (Aldrich), 1,12-dodecanediol (Aldrich), 1,-14-tetradecanediol (Aldrich), 12-bromo-1-dodecanol (Aldrich), hexadecyldisulfide (Lancaster), tetradecyl sulfide (TCI), hexadecyl ether (TCI), stearone (TCI), *trans*-17-pentatriacontene (Aldrich), 7-hexadecyn-1-ol (Lancaster), and dioctadecylamine (Pfaltz & Bauer) are commercially available and were used as received. The molecules containing fluoro, chloro, iodo, and nitrile groups were synthesized as described below.[22]

Synthesis of $CF_3(CF_2)_3(CH_2)_{10}OH$. After flushing with nitrogen, perfluorobutyl iodide, 9-decen-1-ol, and a catalytic amount of azobisisobutyronitrile, AIBN, were added to an ampule fitted with a Teflon stopcock. The ampule was sealed and heated to 70 °C for 24 h. The resulting solution was transferred to a flask equipped with a condenser and a catalytic amount of AIBN. After heating to 60 °C, tributyltin hydride was added over a period of 40 min, and the solution was allowed to stir for 4 h. Multiple distillations at 164 °C and 3 mmHg gave the desired product. ^{1}H NMR ($CDCl_3$): 1.39 (s, 14 H), 1.58−1.69 (m, 2 H), 1.98−2.18 (m, 2 H), 2.34 (s, 1 H), 3.65 (t, 2 H). ^{13}C NMR ($CDCl_3$): 13.4, 16.8, 20.1, 26.7, 27.1, 28.8−28.9 (m, 2 C), 31.8−32.0 (m, 1 C), 33.2, 63.6, 120.8 (m, 4 C). Anal. Calcd. for $C_{14}H_{21}F_9O$: C, 44.68; H, 5.63. Found: C, 44.33; H, 6.12.

Synthesis of $CF_3(CH_2)_{11}OH$. Using a similar procedure, an ampule was filled with undecylenyl alcohol, trifluoromethyl iodide, and a catalytic amount of AIBN. The ampule was sealed and heated to 70 °C for 24 h. The resulting solution was transferred to a flask equipped with a condenser and a catalytic amount of AIBN. After heating to 60 °C, tributyltin hydride was added over a period of 40 min and the solution was allowed to stir for 4 h. Multiple distillations at 50 mmHg and 86 °C gave the desired product, mp 27 °C. ^{1}H NMR ($CDCl_3$): 1.38 (s, 22 H), 1.58−1.62 (m, 2 H), 1.78 (s, 1 H), 2.02−2.21 (m, 2 H), 2.72 (t, 2 H). Anal. Calcd. for $C_{12}H_{23}F_3O$: C, 59.98; H, 9.65. Found: C, 58.21; H, 9.17.

Synthesis of $Cl(CH_2)_{12}OH$. A 2 g sample of 1,12-dodecanediol was refluxed for 24 h in the presence of petroleum ether (2 mL) and concentrated HCl (26.3 mL). Petroleum ether (13 mL) was then added to the hot reaction mixture, and the organic layer was removed. Another 10 mL of petroleum ether

was added to the reaction mixture, and the organic layer was removed and combined with the previous extract. The combined extract was cooled, and the precipitated diol was removed. Distillation of the resulting oil at 2 mm Hg and 95 °C gave the dichloride, and the desired product was collected at 2 mm Hg and 100 °C. ^{1}H NMR ($CDCl_3$): 1.38 (s, 16 H), 1.53−1.64 (m, 2 H), 1.78−1.89 (m, 2 H), 3.58 (t, 2 H), 3.72 (t, 2 H). Anal. Calcd. for $C_{12}H_{25}ClO$: C, 65.28; H, 11.41. Found: C, 64.29; H, 11.48.

Synthesis of $I(CH_2)_{12}OH$. A 1 g sample of 12-bromododecanol was dissolved in 25 mL of butanone. A 0.75 g sample of NaI was added to this solution, and the mixture was refluxed for 1 h. The mixture was then filtered and the solvent removed. The product was purified by dissolving in pentane, removing the solvent, and filtering the resulting solid. ^{1}H NMR ($CDCl_3$): 1.38 (s, 16 H), 1.56−1.68 (m, 2 H), 1.81−1.95 (m, 2 H), 3.22 (t, 2 H), 3.72 (t, 2 H). Anal. Calcd. for $C_{12}H_{25}IO$: C, 46.16; H, 8.07. Found: C, 46.21; H, 8.12.

Synthesis of $NC(CH_2)_{12}OH$. In a three-necked flask, 1 mL of water was added to 0.96 g of NaCN, and the solution was heated until the mixture dissolved. A solution of 12-bromododecanol in 50 mL of methanol was added to the NaCN solution over a period of 5 min, and the mixture was refluxed for 24 h. The solvent was removed and the product was purified by column chromatography (30% ethyl acetate, 70% hexane). ^{1}H NMR ($CDCl_3$): 1.37 (s, 16 H), 1.40−1.51 (m, 2 H), 1.64−1.77 (m, 2 H), 2.39 (t, 2 H), 3.69 (t, 2 H). ^{13}C NMR ($CDCl_3$): 17.7, 36.1, 36.7, 38.0, 39.7, 43.6, 63.9, 120.4. Anal. Calcd. for $C_{13}H_{25}NO$: C, 73.88; H, 11.92; N, 6.63. Found: C, 73.94; H, 11.86; N, 6.57.

III. Results

1. STM Images of Alkanes and Alkanols. Figure 1a−c displays representative STM images for three different molecular monolayers on highly ordered pyrolytic graphite: $C_{10}H_{21}OH$, $C_{12}H_{25}OH$, and $C_{14}H_{29}OH$. For comparison, Figure 1d displays a representative STM image obtained, under nominally identical conditions, from a monolayer of pentatriacontane ($C_{35}H_{72}$) adsorbed on graphite. These images were highly reproducible under our conditions and are representative of the many hundreds of images obtained of these monolayers over numerous independent trials.

The prominent features of these images clearly can be assigned to the structure of the molecules in the graphite overlayer. In each case, lamellae were observed. In images of the alkane and alkanol overlayers, molecules in adjacent lamellae are staggered by half of the molecular width.[14,21] The metrics of interest in the images are schematically indicated in Figure 1e. Figure 1f shows average line scans for these three images taken perpendicular to the lamellae. The mean length, *a*, of the lamellae was 26.7, 32.4, and 38.0 (±0.5) Å for the C_{10}, C_{12}, and C_{14} alkanol overlayer, respectively. For the overlayer derived from the $C_{35}H_{72}$ alkane, the lamellae had a mean length of 47.5 ± 0.5 Å, while those of $C_{36}H_{74}$ had a mean length of 48.8 ± 0.5 Å. The mean molecular lengths of 14.7, 17.6, and 19.9 Å for the C_{10}, C_{12}, and C_{14} alkanols, respectively, and 47.5 Å for $C_{35}H_{72}$ and 48.8 Å for $C_{36}H_{74}$ correspond quite well with the lengths of the all-*trans*-conformations that are calculated using the standard bond length values and van der Waals radii for the terminal atoms of these molecules. These lengths are 14.1, 16.7, and 19.2 Å for the C_{10}, C_{12}, and C_{14} alkanols, respectively, and 45.4 Å for $C_{35}H_{72}$ and 46.7 Å for $C_{36}H_{74}$. Aditionally, the unit cell dimensions determined from the STM data are in excellent agreement with the unit cell dimensions observed in previous low-angle X-ray diffraction studies of alkanol monolayers on graphite (Table 1).[21]

The lamellae of the alkanol overlayers were observed to form a herringbone structure. In the STM images, the angle θ of Figure 1e was 23°, 24°, and 25° for decanol, dodecanol, and tetradecanol, respectively, compared to an orientation angle determined by X-ray diffraction methods of ∼26° for alkanol monolayers on graphite.[21] The herringbone structure of the alkanol overlayer is consistent with expectations based on hydrogen-bonding interactions driving the intermolecular packing geometries of these systems. The distance *d* between molecules determined from the X-ray diffraction data was 4.5−4.6 Å,[21] and that from STM data was 4.4−4.6 Å. The STM observations are thus in excellent agreement with the low-angle X-ray diffraction data on these overlayers, lending confidence to the assignments of the STM images described herein.

The molecular-resolution features described above are similar to the qualitative features of STM images of related alkane or alkanol molecular overlayers that have been reported previously.[12−19] In this work, additional important information was obtained from a detailed analysis of higher resolution STM images. These highly resolved images were repeatable, but not always predictable. Higher magnification images (Figure 2a) of a representative alkanol containing 14 carbon atoms in its backbone, $C_{14}H_{29}OH$, showed that each molecule exhibited 14 alternating bright spots that were separated by a mean distance of 2.57 ± 0.02 Å in the direction along the molecule (a to b). The angle between adjacent bright spots (angle acb) in an individual molecule was measured to be 61°, and the distance between these spots was 2.36 ± 0.02 Å (a to c and b to c). In addition, the distance between alternating spots in adjacent molecules was 2.76 ± 0.02 Å (c to d).

These distances do not correspond to the lattice spacing of the underlying graphite substrate. Specifically, the distance between adjacent β site carbon atoms in a graphite lattice is 2.46 Å, and that between β site carbon atoms located in every second carbon row of the graphite structure is 4.26 Å.[23] The origin of the bright spots in the STM data therefore cannot be explained in terms of enhanced imaging of graphite lattice atoms by the presence of the adsorbed alkanol, since any orientation of an alkanol having the overlayer commensurate with certain graphite atoms (to match some of the observed spot positions) would produce equivalently imaged spots in positions that cannot be overlaid onto any corresponding graphite lattice atom or lattice site. Additionally, the spots cannot be attributed to the carbon atoms in the adsorbed tetradecanol molecules because the separations and angles observed for the spots do not correspond well to the expected C−C distance and angle of 1.55 Å and 109.5° for a *trans*-alkane.[24] The observed distances do, however, correspond closely to the H−H distances expected for hydrogens attached to adjacent (2.52 Å) and next-nearest (2.56 Å) methylene units in *trans*-alkanes.[24] The measured bond angle of 61° between adjacent spots in an alkanol lamella is also in accord with the H−H angles of 61.3° expected for hydrogens on adjacent methylene units in a *trans*-alkane. Thus, the metrics obtained from the experimental data indicate that the bright spots in individual alkanol molecules are primarily related to the locations of the individual hydrogen atoms on the methylene units of an alkanol chain. This assignment also implies that the plane containing the carbon−carbon skeleton in the alkanols lies in an orientation parallel to the graphite surface plane (Figure 2b).

Low-resolution images of alkanes exhibited bright spots that appeared to be associated with alternating methylene units in the alkane chain. For example, images of $C_{35}H_{72}$ showed 17 spots of mean separation 2.57 ± 0.02 Å (Figure 1d). These images are in accord with the images of alkane overlayers on graphite presented previously in the literature.[12,14] However,

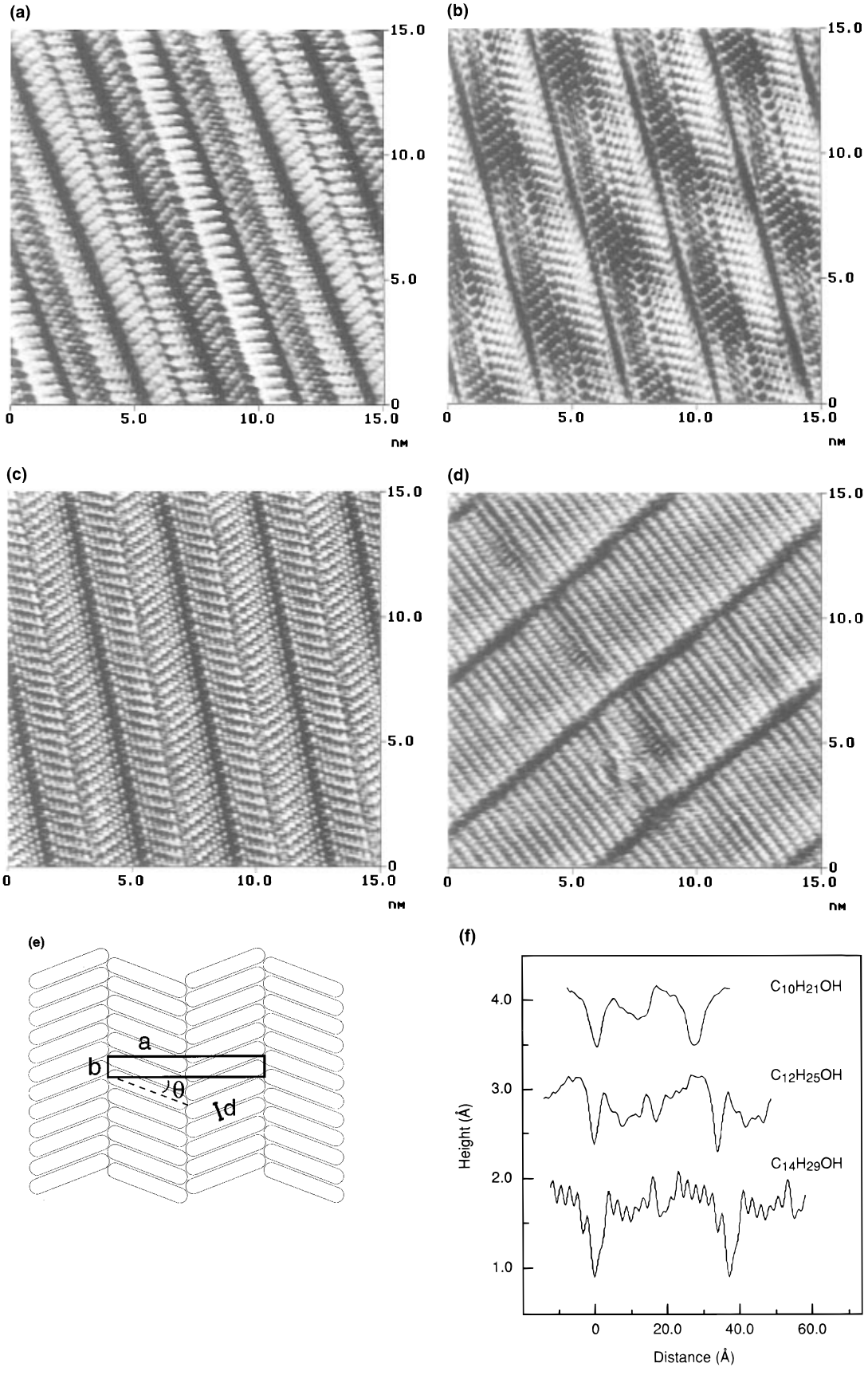

Figure 1. (a) Constant current STM image of a monolayer of decanol ($C_{10}H_{21}OH$) molecules adsorbed on a graphite surface ($V = 1.015$ V, $I =$ 650 pA, line direction = left, frame direction = down). (b) STM image of a monolayer of dodecanol ($C_{12}H_{25}OH$) molecules adsorbed on graphite ($V = 1.210$ V, $I = 650$ pA, line direction = down, frame direction = left). (c) STM image of a monolayer of tetradecanol ($C_{14}H_{29}OH$) molecules adsorbed on graphite ($V = 1.127$ V, $I = 650$ pA, line direction = right, frame direction = up). (d) STM image of a monolayer of pentatriacontane ($C_{35}H_{72}$) molecules on graphite ($V = -1.611$ V, $I = 650$ pA, line direction = left, frame direction = down). The images are dominated by the structure of the adsorbate molecules and clearly show the herringbone structure of the alcohol monolayers and the parallel packing structure of the alkane monolayer. (e) Schematic diagram depicting the unit cell of an alkanol monolayer on graphite. (f) Averaged line scans across the lamellae for decanol, dodecanol, and tetradecanol monolayers. As expected, the size of the lamellae increases with increasing chain length of the adsorbed molecules.

TABLE 1

	unit cell by STM		unit cell by X-ray diffraction[21]	
molecule	*a* (Å)	*b* (Å)	*a* (Å)	*b* (Å)
$C_{10}H_{21}OH$	26.7 ± 0.5	5.0 ± 0.2	26.5 ± 0.3	5.17 ± 0.02
$C_{12}H_{25}OH$	32.4 ± 0.5	5.2 ± 0.2	32.0 ± 0.4	5.04 ± 0.02
$C_{14}H_{29}OH$	38.0 ± 0.5	5.2 ± 0.2		

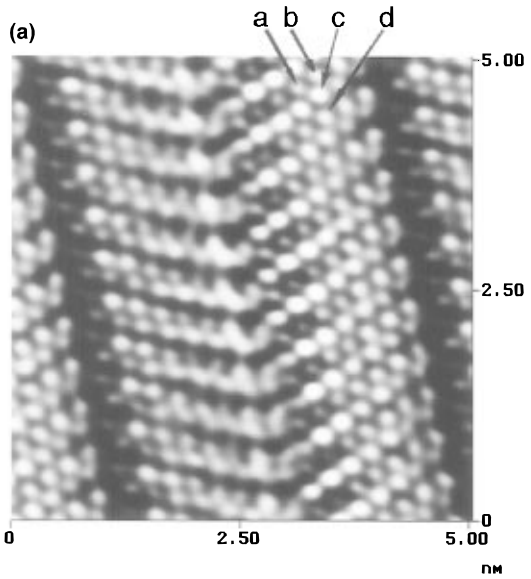

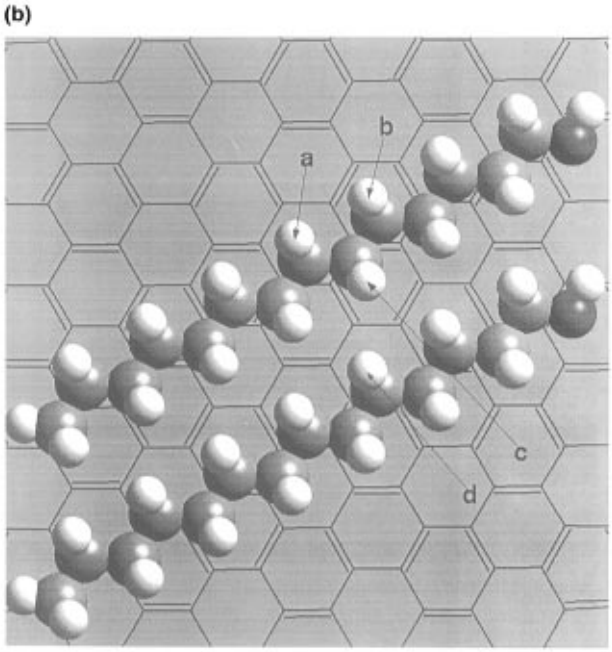

Figure 2. (a) High-resolution STM image of tetradecanol molecules on graphite ($V = 1.127$ V, $I = 650$ pA, line direction = right, frame direction = up). Individual tetradecanol molecules produce 14 bright spots in the STM image which correspond closely to the locations of the 14 hydrogen atoms nearest to the tip. (b) Schematic diagram of individual tetradecanol molecules adsorbed onto graphite.

high-resolution STM images of the alkanes (Figure 3), which were obtained using nominally the same experimental parameters as those that produced the lower resolution images, displayed alternating spot patterns that are very similar to those observed in the alkanol images. Images of $C_{35}H_{72}$ displayed bright spots that are separated by a mean distance of 2.54 ± 0.02 Å in the direction along a molecule (a to c) and by a distance of 2.35 ± 0.02 Å between adjacent spots within a molecule (a to b and b to c). These data are nearly identical to those for the alkanol overlayers and indicate that the positions

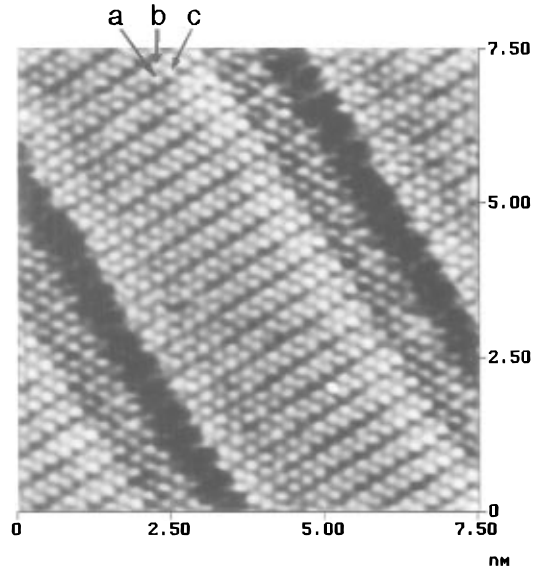

Figure 3. High-resolution STM image of pentatriacontane molecules on graphite ($V = 1.210$ V, $I = 650$ pA, line direction = left, frame direction = down). Unlike the lower resolution image in Figure 1d that seems to show every other methylene group (17 bright spots), the high-resolution image shows 35 bright spots, which correspond closely to the positions of the 35 upward-facing hydrogen atoms in the alkane chain. Similar to the alkanol overlayers, the molecules appear to be oriented with their carbon−carbon skeleton parallel to the graphite surface plane. The slight variation in contrast visible along the alkane chains was observed to be very tip dependent and changed with time.

of the bright spots in images of the alkanes are dominated by the locations of individual hydrogen atoms on methylene units in a *trans*-alkane chain. These metrics also imply that the alkanes, like the alkanols, are adsorbed under our imaging conditions such that the bonds in the carbon−carbon skeleton are oriented in a plane parallel to the graphite surface. These high-resolution images of the alkanes appear to be in accord with a previously published STM image of a $C_{36}H_{74}$ overlayer on graphite,[25] but a detailed determination of the important metrics of high-resolution STM images of alkane overlayers such as that described above has not, to our knowledge, been reported previously in the literature.

Many of the STM images for the alkanes and alkanol overlayers also contained a larger scale modulation of the image contrast. This regular modulation in the image contrast is likely due to a Moiré pattern between the lattices of the graphite and of the monolayer.[26,27] In fact, this pattern changes as the chain length of the molecule changes, and it is also a function of bias voltage and tip condition (vide infra). As a result of this superstructure, the contrast of the bright regions assigned to the hydrogen atoms sometimes varied slightly from one end of a molecule to the other.[28] Moiré patterns can arise from the presence of two or more monolayers of an organic species adsorbed onto a substrate,[29] but prior calorimetric and X-ray diffraction data indicate that only single monolayers of alkanes and alcohols are absorbed onto graphite from the dilute solutions of these adsorbates that were used in our work.[21]

2. STM Images of Diols. The molecular resolution STM image of dodecanol displayed in Figure 1b is similar to other alkanol images reported previously[12,15,16] and does not allow immediate identification of the location of the OH group in the alkanol. The dark trough of mean length 4.3 ± 0.1 Å that seemingly separates each lamella, corresponding to a 0.46 ± 0.05 Å tip−sample decrease (relative to the average methylene height) required to maintain a constant 650 pA current at a sample bias of +1.210 V, could either contain two OH groups hydrogen-bonded to each other or could be the site of two

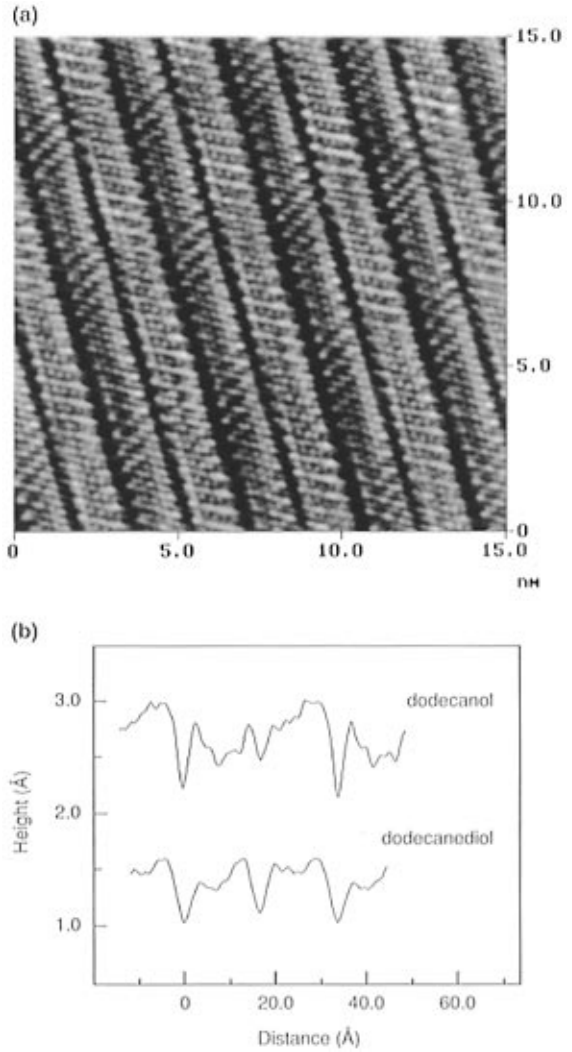

Figure 4. (a) STM image of a 1,12-dodecanediol monolayer on graphite ($V = 1.318$ V, $I = 650$ pA, line direction = left, frame direction = up). Unlike the image of dodecanol in Figure 1b, in which troughs are apparent on only one side of the molecules, in this image identical troughs are visible on both sides of the diol molecules. (b) Averaged line scans taken perpendicular to the lamellae (parallel to the *a* axis of the unit cell) for dodecanol and dodecanediol. Note that twice as many troughs are apparent in the line scan of dodecanediol as compared to dodecanol. This comparison shows that the hydroxyl functionalities are dark relative to the methylene groups, i.e. have a lower tunneling probability relative to the methylene groups in the alkane chain.

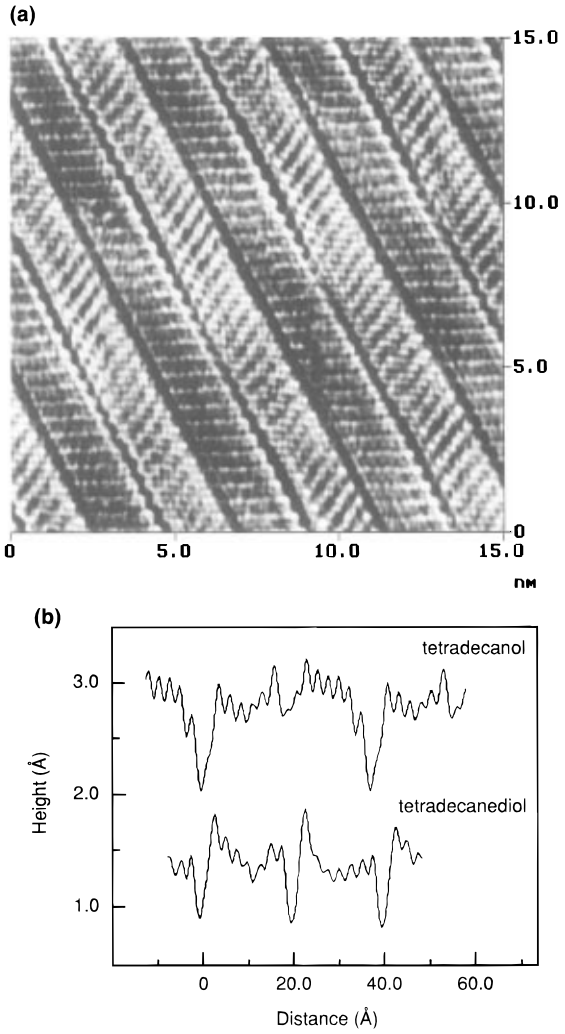

Figure 5. (a) STM image of 1,14-tetradecanediol molecules on graphite ($V = 1.095$ V, $I = 650$ pA, line direction = down, frame direction = right). Troughs are apparent at both ends of the molecules, as compared to only in one side for tetradecanol (Figure 1c), indicating that the hydroxyl groups are dark relative to the methylene groups in the alkane chain. (b) Averaged line scans taken perpendicular to the lamellae (parallel to the *a* axis of the unit cell) for tetradecanol and tetradecanediol. Note that twice as many troughs are apparent in the line scan of tetradecanediol as compared to tetradecanol.

terminal CH_3 groups, one on each alkanol chain. However, since the positions of the individual spots were assigned in this work to be dominated by the locations of H atoms on methylene units in the alkanol chains, and since high-resolution images of the alkanols showed no troughs between molecules on one side and troughs on the other (Figure 2), it is very reasonable to associate these troughs with the location of the OH groups.

To validate this hypothesis without relying on such spot assignments, STM data were collected on overlayers of α,ω-alkanediols on graphite and the images compared to those of the corresponding alcohol. Figure 1b shows a STM image of dodecanol, and Figure 4a displays an image of the corresponding diol, $HO(CH_2)_{12}OH$. The image of the diol exhibits lamellae of mean length of 34.5 ± 0.5 Å, as compared to a mean lamellar length of 32.4 ± 0.5 Å for dodecanol (Figures 4b and 1f). Identically sized troughs are apparent at both ends of the molecules in the dodecanediol image, with the troughs having an average width of 4.3 ± 0.1 Å and an average depth of 0.42 ± 0.05 Å. Since the trough at the end of the dodecanol molecule is identical to the dark regions at the terminal areas of the diol molecules, these dark regions can be clearly assigned to OH groups.

A similar comparison was performed between the STM images of tetradecanol and 1,14-tetradecanediol (Figures 1c and 5a). The mean length of the lamellae in images of tetradecanol was 38.0 ± 0.5 Å, while the mean lamellar length in images of 1,14-tetradecanediol was 39.3 ± 0.5 Å (Figure 1f and 5b). The trough at the end of the molecule in the image of tetradecanol had a mean length of 4.3 ± 0.1 Å and a mean depth of 0.82 ± 0.05 Å. As was the case for images of $HO(CH_2)_{12}OH$, the troughs at both ends of the lamellae in the images of 1,14-tetradecanediol were identical, having an average length of 4.1 ± 0.1 Å and an average depth of 0.61 ± 0.05 Å. These data are also consistent with the assignments made above regarding the location of the hydroxyl functionality and suggest that, in general, hydroxyl groups in alkanols will appear dark, i.e., will comprise regions of lower tunneling probability relative to methylene or methyl units in an alkane chain. The data also clearly show, contrary to earlier suggestions in the literature, that OH groups can be distinguished by STM methods from terminal methyl groups in images of alkanol overlayers on graphite.[16,20]

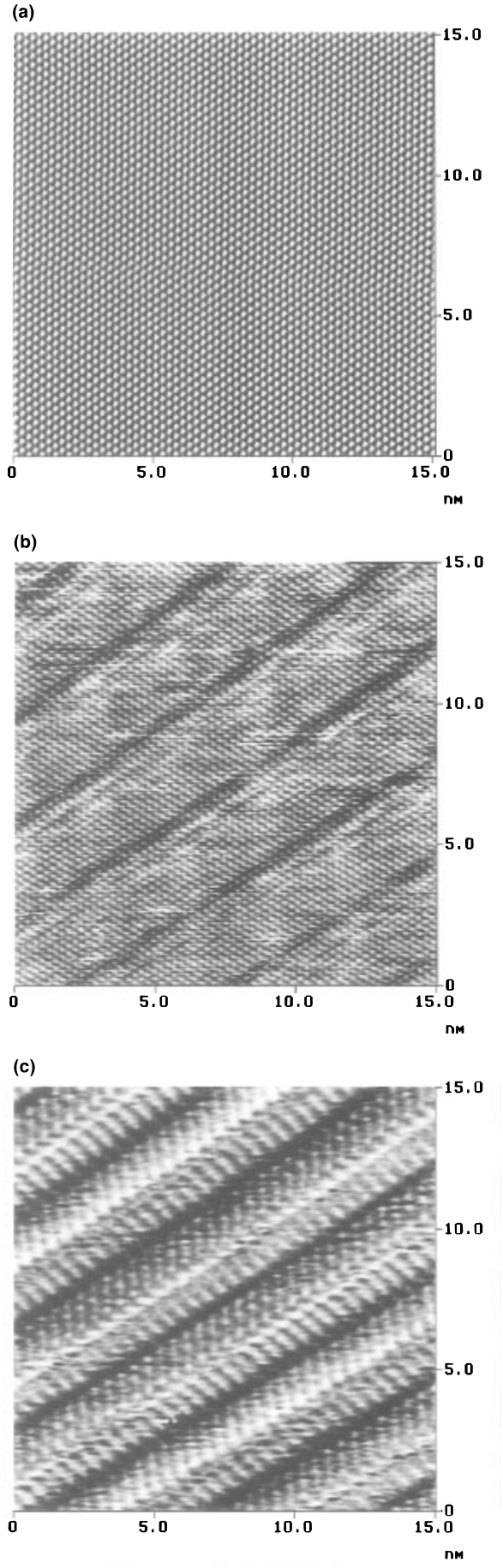

Figure 6. STM images of decanol on graphite. (a) The STM image is dominated by the substrate at low bias ($V = 0.050$ V, $I = 660$ pA, line direction = left, frame direction = up). (b) At an intermediate bias, the image is comprised of features associated with both the substrate and the adsorbate ($V = 0.855$ V, $I = 433$ pA, line direction = left, frame direction = down). (c) At high biases, the image is dominated by the adsorbate ($V = 1.160$ V, $I = 574$ pA, line direction = left, frame direction = down).

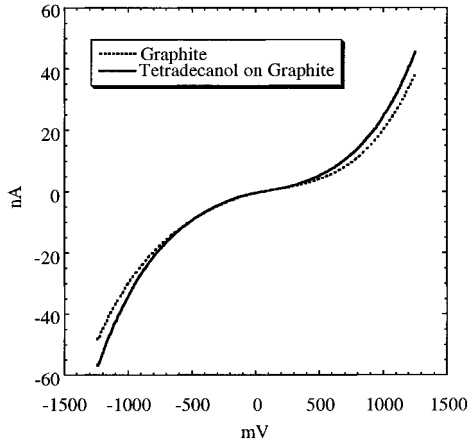

Figure 7. *I*/*V* curves of graphite and tetradecanol adsorbed on graphite with the tip−sample separation defined by a sample bias of 100 mV and setpoint current of 650 pA.

3. Bias Dependence of the STM Images of Alkanes and Alkanols on Graphite. In accord with other reports in the literature,[12,14,15,18,19] we have observed that the image contrast for alkanes and alkanols adsorbed on graphite depends on the tunneling bias. Figure 6a−c shows a series of STM images of decanol adsorbed on graphite as a function of bias voltage that were obtained over the same spatial region of the graphite surface. At low bias (i.e., at a tunnel gap resistance $R_{gap} = V/i = 76$ MΩ), the STM height image is dominated by the graphite substrate. At an intermediate bias voltage ($R_{gap} = 1975$ MΩ), the height image is comprised of features that can be associated with a combination of the substrate and adsorbate. At high biases, generally 1 V in magnitude ($R_{gap} = 2020$ MΩ), the height image is dominated mostly by the adsorbate, and the herringbone structure of the decanol molecules is clearly observed. The transition between these various images was observed for several runs and was independent of the sequence in which the data were collected; only the bias voltage and setpoint current determined which image was observed over a specific region of the sample. During the course of this study, we never reproducibly observed a "contrast reversal" during, or between, successive STM scans, in which the features in an image spontaneously reversed in contrast and could then be reproducibly imaged in this other image format. The simultaneous observation of features that can be associated with both the molecule and the graphite surface structure (Figure 6b) strongly suggests that the observed bias dependence of the images is not predominantly a result of physical displacement of molecules from the substrate by the tip at low or intermediate bias voltages. The data of Figure 6b also reveal that the decanol lamellae in the overlayer are aligned with the underlying graphite lattice.

The bias dependence of the images was observed not to depend on the polarity of the bias voltage; the bias dependence was thus symmetrical about 0 V between the tip and sample. Figure 7 shows *I*/*V* curves for the bare graphite surface and for the adsorbate-covered surface. The curves are antisymmetrical with respect to bias polarity, and the tunneling current observed for the adsorbate-covered surface increases slightly more rapidly with bias than for the bare graphite surface (Figure 7). The dependence of image contrast on bias is not unique to alkanes and alkanols adsorbed onto graphite; it has also been observed for phthalocyanine molecules,[30] cytochrome c_3,[31] and a variety of liquid crystals.[32,33] However, it is especially interesting to

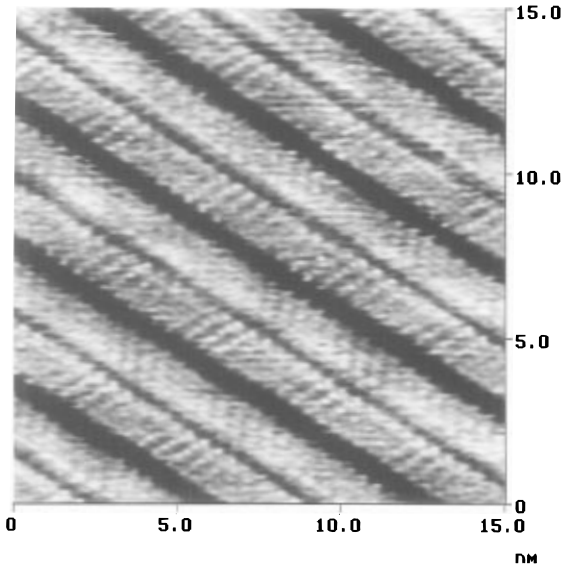

Figure 8. STM image of $CF_3(CH_2)_{11}OH$ molecules on graphite ($V = -0.410$ V, $I = 650$ pA, line direction = left, frame direction = down). The smaller trough is assigned to the OH groups, while the larger trough is assigned to the regions containing terminal CF_3 groups.

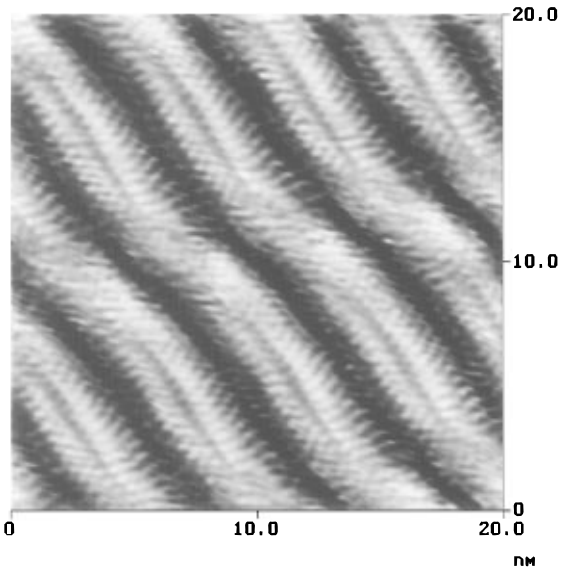

Figure 9. STM image of $CF_3(CF_2)_3(CH_2)_{10}OH$ molecules on graphite ($V = 0.185$ V, $I = 650$ pA, line direction = right, frame direction = down). The smaller trough is assigned to the OH groups, while the larger trough is assigned to the regions containing terminal $CF_3(CF_2)_3$ groups. Like the hydroxyl group, fluorinated groups are found to be dark relative to the methylene groups.

note that the images were essentially symmetrical with respect to the zero bias position, set in this case by the Fermi level of the graphite.

4. STM Images of Alkanols with Perfluorinated Methyl and Methylene Functionalities. Since prior calorimetry measurements have shown that alkanols exhibit significantly more negative enthalpies of adsorption on graphite than the corresponding alkanes,[11] further STM data were collected on functionalized alkanols generally having 10−14 carbons in the alkane chain. The use of substituted alkanols having terminal hydroxyl groups allowed reproducible preparation of ordered monolayers of the molecular species on the graphite surface. In addition, the presence of the terminal hydroxyl group served as a convenient reference for establishing the relative contrast of other functional groups in the STM data. The section below describes STM images of alkanols that contain perfluorinated methyl and/or perfluorinated methylene groups.

We were unable to observe STM images of completely fluorinated alkanols such as hexadecafluoro-1,10-decanediol, most likely because a crystalline monolayer is not formed at room temperature on the graphite substrate. We did, however, observe STM images for partially fluorinated alkanols on graphite substrates. A STM image of $CF_3(CH_2)_{11}OH$ on highly ordered pyrolytic graphite is shown in Figure 8. The average length of the lamellae is 33.6 ± 0.5 Å, and the average molecular length is 17.9 ± 0.5 Å. This mean molecular length is in good agreement with the molecular length of 17.2 Å obtained from molecular modeling using Cerius 2 software for the all-*trans*-conformation of the molecule. Troughs were apparent at both ends of the molecules, with one trough being longer and deeper than the other. The smaller trough has a width of 3.9 ± 0.1 Å and a depth of 0.49 ± 0.5 Å, and this is assigned to the OH groups due to its similarity to the troughs observed in STM images of alkanols and alkanediols (Figures 4 and 5). The larger trough, assigned to the regions containing CF_3 groups, has an average width of 8.2 ± 0.1 Å and depth of 1.32 ± 0.05 Å. Thus, like the OH functionality, the CF_3 group is dark relative to the methylene groups. The contrast in the images of this molecule was similar at positive and negative sample biases, as was observed for the alkanes and alkanols.

Figure 9 shows the STM image of $CF_3(CF_2)_3(CH_2)_{10}OH$ at positive sample bias. The image is not as clearly resolved as images of the alkanol molecules described above, and this may be due to the dynamics of the fluorinated ends of the molecule in these room-temperature images (which may also explain the large width of the CF_3 regions in the images of Figure 8). Lamellae of mean length 38.8 ± 0.5 Å are observed, and the average length of the molecules is 19.9 ± 0.5 Å. This length is in excellent agreement with the length of 19.8 Å for the all-*trans*-conformation of this molecule obtained from molecular modeling. Additionally, the STM images showed dark regions of mean length 4.3 ± 0.1 Å and depth 0.30 ± 0.05 Å that are assigned to the OH groups. The longer trough can be assigned to the fluorinated region of the molecule and has an average length of 16.0 ± 0.5 Å and a mean depth of 1.32 ± 0.05 Å. The large-scale periodicity in the image is likely due to a packing effect or to a Moiré pattern between the monolayer and substrate. As was the case for the OH group, we conclude that the fluorinated part of the molecule is dark relative to the methylene groups in such STM images at both positive and negative sample bias.

5. STM Images of Alkanol Halides. This approach was readily extended to a variety of functional groups. Figures 10−12 display representative STM data for the halides 12-bromo-1-dodecanol, $Br(CH_2)_{12}OH$, 12-chloro-1-dodecanol, $Cl(CH_2)_{12}$-OH, and 12-iodo-1-dodecanol, $I(CH_2)_{12}OH$; the topographic metrics of these images are summarized in Table 2. Similar to the previous molecules, the STM contrast of the functional groups was independent of the bias polarity. The STM image of 12-bromo-1-dodecanol, $Br(CH_2)_{12}OH$, at negative sample bias is shown in Figure 10. The average length of the molecules in the 12-bromo-1-dodecanol overlayer is 17.8 ± 0.3 Å, which compares well with the predicted length obtained from molecular modeling of 17.5 Å for an all-*trans*-conformation of this molecule. Dark regions are observed on both ends of the molecule, indicating that bromine, like fluorine and oxygen, is dark relative to the methylene groups of these overlayers. A recent STM study of 1-bromodocosane (n-$C_{22}H_{45}Br$) adsorbed on graphite observed that the bromide functionality was generally dark in contrast relative to the alkyl chain,[20b] in accord with our data for $Br(CH_2)_{12}OH$. However, the STM images of $C_{22}H_{45}Br$ did not allow unambiguous identification of location of the Br group.[20b] The use of brominated alkanols, which

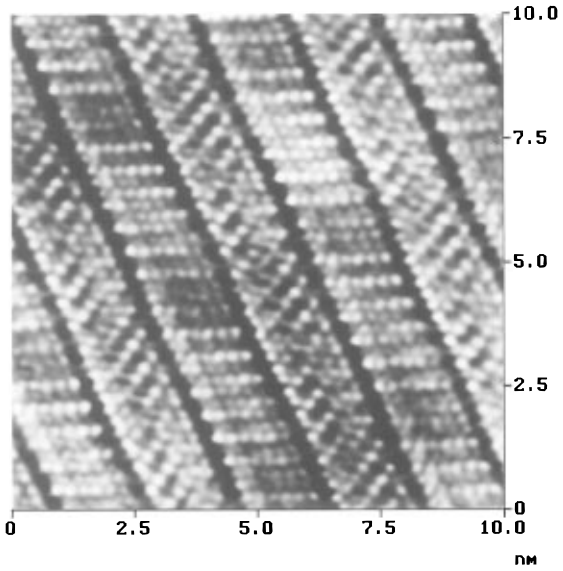

Figure 10. STM image of $Br(CH_2)_{12}OH$ molecules on graphite ($V = -1.243$ V, $I = 650$ pA, line direction = right, frame direction = up). Similar troughs are located at both ends of the molecules, indicating that the bromine is dark relative to the methylene groups.

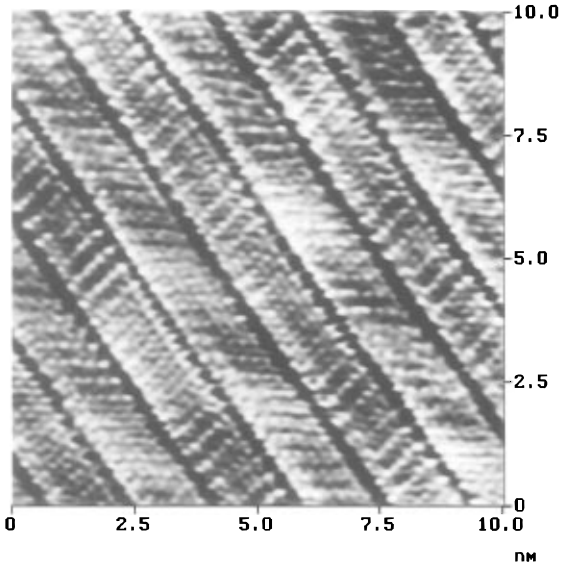

Figure 11. STM image of $Cl(CH_2)_{12}OH$ molecules on graphite ($V = 1.095$ V, $I = 650$ pA, line direction = right, frame direction = up). Similar to 12-bromo-1-dodecanol, both ends of the molecules are dark, indicating that the chlorine is dark relative to the methylene groups.

adsorb more strongly onto graphite than brominated alkanes, enables higher resolution STM images to be obtained and permits location of the Br functionality through reference to the position of the characteristic OH trough in the STM images of subustituted alkanols. Thus, for $Br(CH_2)_{12}OH$, the metrics of the STM images in positive bias allowed differentiation between the position of the OH group and that of the Br functionality (Table 2).

The STM image of 12-chloro-1-dodecanol, $Cl(CH_2)_{12}OH$, also shows dark troughs on either side of the molecule, indicating that chlorine is dark as well (Figure 11). Under the imaging conditions of this work, the locations of the Cl groups could not be distinguished from those of the OH functionalities. The average length of the molecules in the 12-chloro-1-dodecanol overlayer is 17.3 ± 0.3 Å, which is in excellent agreement with the length of 17.4 Å predicted for the all-*trans*-conformation of this molecule by molecular modeling. The STM image of 12-iodo-1-dodecanol, $I(CH_2)_{12}OH$, is shown in Figure 12. The average length of the molecules is 18.1 ± 0.3 Å, as compared with the predicted length of 17.8 Å from molecular modeling of the all-*trans*-conformation. Unlike the previous molecules described above, images of this molecule show a slightly different packing arrangement and reveal that one end is dark while the other is bright. Knowing that the OH functionality is dark, we logically conclude that the iodine-containing regions are bright relative to the methylene groups in such STM images. This conclusion is in accord with recent STM images of 1-iodooctadecane on graphite, which also display bright iodide groups relative to the alkyl portions of the molecular overlayer.[20b]

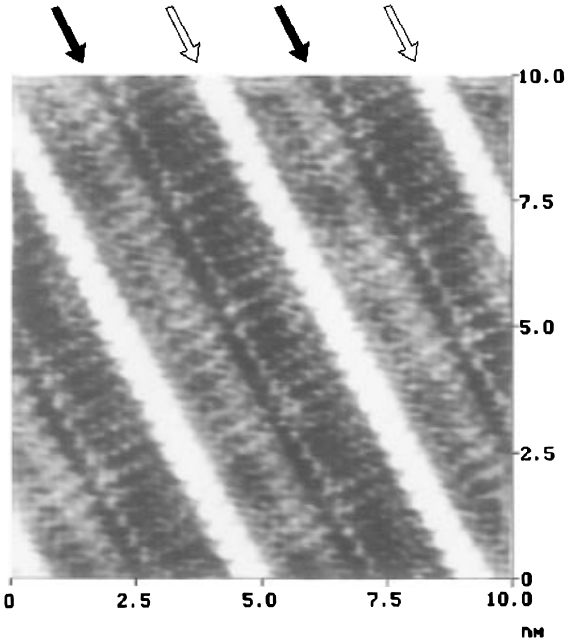

Figure 12. STM image of $I(CH_2)_{12}OH$ molecules on graphite ($V = -0.177$ V, $I = 650$ pA, line direction = right, frame direction = down). Using the dark trough associated with the terminal hydroxyl groups as a reference (black arrows), the bright region at the other end of the molecules is assigned to the region containing the iodine heteroatoms (white arrows).

6. Disulfides, Thioethers, Ethers, and Amines. Figure 13 depicts the STM image of a dialkyldisulfide. Rabe *et al*. have reported a STM image of hexadecyldisulfide, $(C_{16}H_{33})_2S_2$, under positive bias;[28] similar to their report, we have found that hexadecyldisulfide adopts a V-shaped conformation about the sulfur atoms (Figure 13), with the alkyl chains forming an angle of 130°. The mean length of the lamellae is 43.9 ± 0.5 Å. In accord with their report, we observe that the sulfur atoms are brighter than the methylene groups in positive bias. We

TABLE 2

		OH features		halide features	
molecule	bias	length (Å)	height (Å)	length (Å)	height (Å)
$BrC_{12}H_{24}OH$	(+)	4.4 ± 0.1	-0.42 ± 0.05	5.9 ± 0.1	-0.63 ± 0.05
$BrC_{12}H_{24}OH$	(−)	4.1 ± 0.1	-0.41 ± 0.05	4.1 ± 0.1	-0.41 ± 0.05
$ClC_{12}H_{24}OH$	(+)	4.4 ± 0.1	-0.56 ± 0.05	4.4 ± 0.1	-0.56 ± 0.05
$ClC_{12}H_{24}OH$	(−)	4.7 ± 0.1	-0.63 ± 0.05	4.7 ± 0.1	-0.63 ± 0.05
$IC_{12}H_{24}OH$	(+)	4.3 ± 0.1	-0.80 ± 0.05	9.0 ± 0.1	1.91 ± 0.05
$IC_{12}H_{24}OH$	(−)	3.9 ± 0.1	-0.56 ± 0.05	8.8 ± 0.1	2.06 ± 0.05

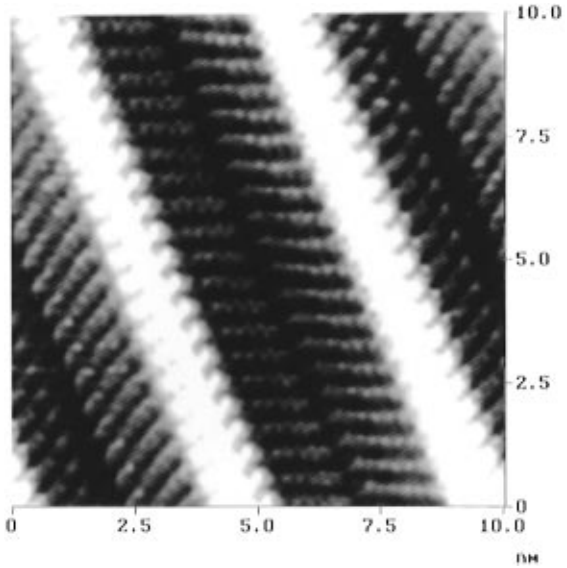

Figure 13. STM image of $(C_{16}H_{33})_2S_2$ molecules on graphite (V = 1.556 V, I = 650 pA, line direction = right, frame direction = down). The disulfide molecules adsorb in a V-shaped conformation about the sulfur atoms, and the sulfur-containing region of the molecule is brighter than the surrounding methylene groups.

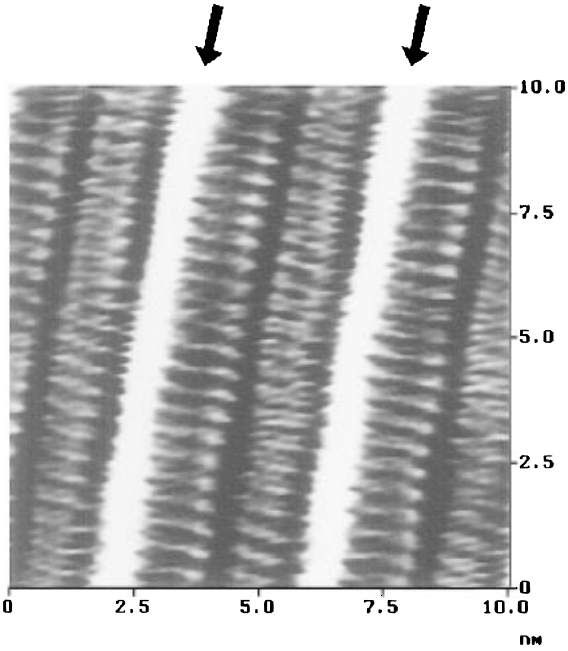

Figure 14. STM image of $(C_{14}H_{29})_2S$ molecules on graphite (V = −1.331 V, I = 650 pA, line direction = left, frame direction = up). The sulfur-containing region in the middle of the molecule is bright relative to the methylene groups (black arrows).

additionally observe the same contrast between the sulfur atom locations and the methylene units for images obtained under negative sample bias.

Figure 14 presents the STM image of a thioether, tetradecyl sulfide, $(C_{14}H_{29})_2S$. The molecule is observed to be linear about the thioether functionality, and the average length of the molecules is 39.2 ± 0.5 Å, as compared to the predicted length of 38.3 Å from molecular modeling. Since the sulfur atoms of the disulfide are brighter than the methylene units (Figure 13), a similar assignment of a bright sulfur-containing functionality can be made for the thioether. This assignment is consistent with recent images of thiols on graphite, in which the terminal SH group was bright compared to the alkyl portion of 1-docosanethiol ($C_{22}H_{45}SH$).[20b] The width of the bright region associated with the thioether functionality was ~7 Å, indicating

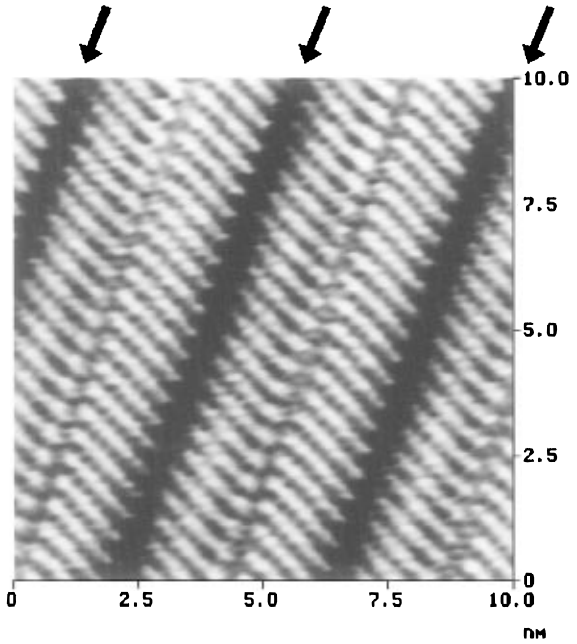

Figure 15. STM image of $(C_{16}H_{33})_2O$ molecules on graphite (V = −1.414 V, I = 650 pA, line direction = right, frame direction = up). Comparison of this image with that of $C_{35}H_{72}$ (Figure 1d) and with the thioether (Figure 14) leads to the conclusion that the dark trough in the middle of the molecular rows is due to the ether functionality (black arrows).

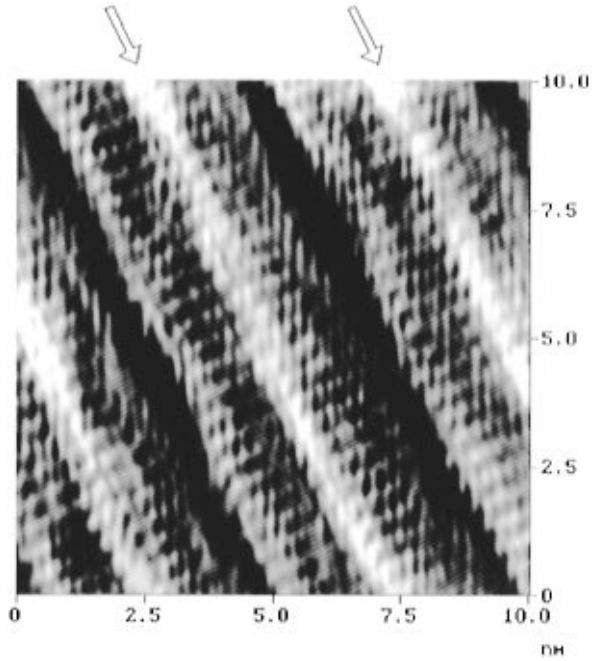

Figure 16. STM image of $(C_{18}H_{37})_2NH$ molecules on graphite (V = 1.331 V, I = 650 pA, line direction = down, frame direction = left). The bright region in the middle of the molecular rows is assigned to the amine group (white arrows).

that the tip height was strongly affected over regions assigned to methylene groups located adjacent to the sulfur atom.

Figure 15 depicts the dramatic change in the image contrast that was observed when the thioether functionality was replaced by an ether functionality, through use of the molecule hexadecyl ether, $(C_{16}H_{33})_2O$. Comparison of the STM image of the ether (Figure 15) with that of tetradecyl sulfide (Figure 14) shows that the ether functionality appears dark relative to the methylene groups. This change in contrast was observed at both positive and negative bias voltages. The molecules were observed to be linear and staggered by half a molecular width across adjacent

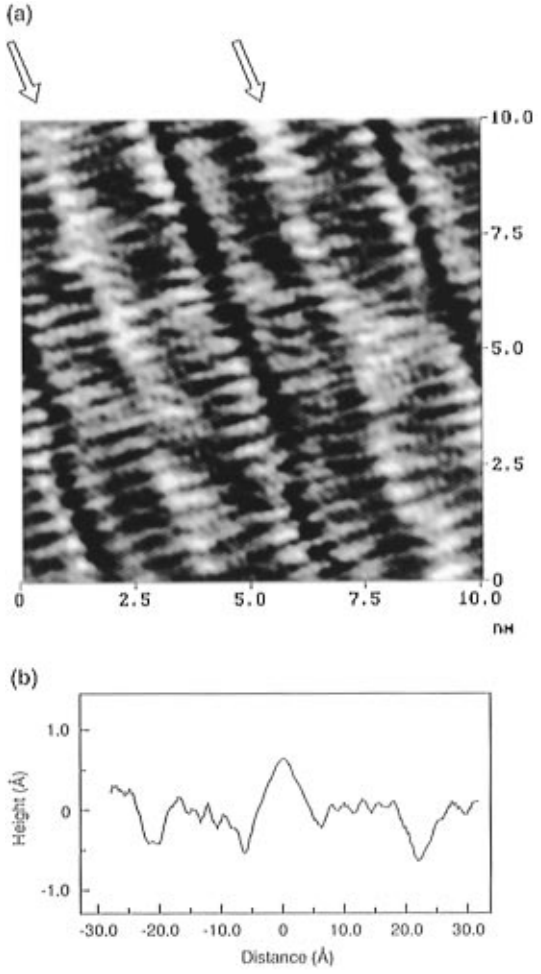

Figure 17. (a) STM image of *trans*-$C_{16}H_{33}HC{=}CHC_{17}H_{35}$ molecules on graphite ($V = 1.193$ V, $I = 650$ pA, line direction = left, frame direction = up). The bright region located toward the center of the molecular rows is assigned to the carbon−carbon double bond (white arrows). (b) Single line scan along the length of the molecule; note the assymetric location of the peak assigned to the double bond relative to the ends of the molecule.

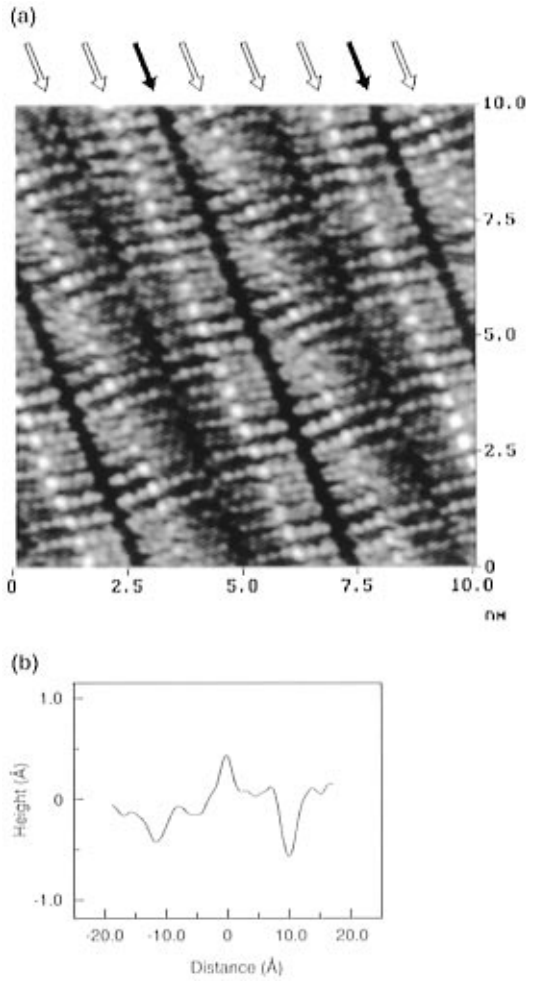

Figure 18. (a) STM image of $H_3C(CH_2)_7C{\equiv}C(CH_2)_6OH$ molecules on graphite ($V = -1.216$ V, $I = 650$ pA, line direction = right, frame direction = up). Using the dark trough associated with the terminal hydroxyl groups as a reference (black arrows), the terminal methyl end of the molecule can be identified (gray arrows), and the bright region located slightly offset from the center of the molecules is assigned to the carbon−carbon triple bond (white arrows). (b) Averaged line scan along the length of the molecules; note the assymetric location of the peak assigned to the triple bond relative to the location of the trough assigned to the OH group.

TABLE 3

		heteroatom features	
molecule	bias	length (Å)	height (Å)
$(C_{16}H_{33})_2O$	(+)	5.5 ± 0.1	-0.74 ± 0.05
$(C_{16}H_{33})_2O$	(−)	5.1 ± 0.1	-0.66 ± 0.05
$(C_{14}H_{29})_2S$	(+)	6.5 ± 0.1	0.80 ± 0.05
$(C_{14}H_{29})_2S$	(−)	6.7 ± 0.1	1.54 ± 0.05
$(C_{16}H_{33})_2S_2$	(+)	11.6 ± 0.1	1.25 ± 0.05
$(C_{16}H_{33})_2S_2$	(−)	12.6 ± 0.1	1.38 ± 0.05
$(C_{18}H_{37})_2NH$	(+)	7.7 ± 0.1	0.54 ± 0.05

lamellae. The average length of the molecules is 43.4 ± 0.5 Å, which compares well with the expected length of 43.0 Å obtained from molecular modeling of the all-*trans*-conformation of hexadecyl ether. The width of the dark, oxygen-containing, region in the ether was ∼5 Å, and, as is the case for most of the other functional groups studied under our conditions, the apparent length of the trough containing the region assigned to the ether functionality is much larger than the expected distance for an oxygen atom, indicating that the tip height is lowered over neighboring methylene groups as well as over the ether functionality itself.

The contrast of an amine functionality is shown in the STM image of dioctadecylamine, $(C_{18}H_{37})_2NH$ (Figure 16). The average length of the molecules is 47.5 ± 0.5 Å, as compared to the expected length of 43.0 Å obtained from molecular modeling of the all-*trans*-form of the amine. This discrepancy is most likely due to drift, which was exacerbated in this image relative to the other images obtained in this work because the amine molecules were aligned in the slow scan direction during this particular experiment. However, we observe the amine group to be bright relative to the methylene groups. This finding is in accord with a recent STM study of 1-octadecylamine ($C_{18}H_{37}NH_2$) overlayers on graphite, in which the amine group was bright relative to the alkyl chain.[20b] The topographic metrics of these functionalities are summarized in Table 3.

7. Alkenes, Alkynes, and Nitriles. We observed a carbon−carbon double bond in the STM image of *trans*-17-pentatriacontene, $C_{16}H_{33}HC{=}CHC_{17}H_{35}$ (Figure 17a). The average length of the molecules is 44.9 ± 0.5 Å, which compares well with the expected length of 45.0 Å obtained from molecular modeling of the all-*trans*-conformation of the molecule. The double bond is located toward the center of the molecule, offset by one carbon, and in the STM image a bright feature appears at both positive and negative bias that is on average 21.8 Å from one end of the molecule and 23.1 Å from the other (Figure 17a,b). Molecular modeling of an all-*trans*-alkane with a *trans*-olefin functionality predicts that the center of the double bond should be located at 21.9 Å from one end of the molecule and 23.1 Å from the other, which compares well with experimental observations. Thus, we conclude that the double bond is bright

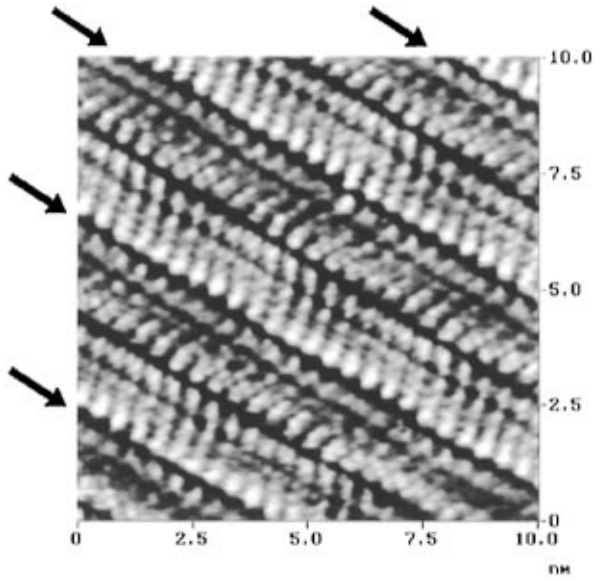

Figure 19. STM image of $HO(CH_2)_{12}C{\equiv}N$ molecules on graphite ($V = -1.421$ V, $I = 650$ pA, line direction = left, frame direction = down). Dark troughs are present on both ends of the molecule, indicating that the nitrile functionality is dark relative to the methylene groups.

in contrast. A carbon−carbon triple bond was observed in the image of 7-hexadecyn-1-ol, $H_3C(CH_2)_7C{\equiv}C(CH_2)_6OH$ (Figure 18), and like the double bond, the triple bond is bright at both positive and negative bias. This observation is in accord with a previous STM image of an alkyne on graphite.[28] The average length of the molecules is 21.6 ± 0.3 Å, which compares well with the expected length of 21.5 Å obtained from molecular modeling of the all-*trans*-conformation of the molecule. The hydroxyl groups are easily identifiable as a trough of length 4.1 ± 0.1 Å and depth 0.49 ± 0.05 Å. The bright feature that is attributed to the triple bond correlates well with its location in the molecule; the feature appears 10.0 Å from the −OH end of the molecule and 11.6 Å from the methyl-terminated end (Figure 18a,b). For comparison, molecular modeling of an all-*trans*-alkane conformation with an internal C−C triple bond indicates that the center of the triple bond should be 10.0 Å from the −OH end of the molecule and 11.5 Å from the methyl-terminated end of the molecule. In addition, the alkyl chains of the molecule are expected to have a kink about the linear C−C triple bond that should be observed experimentally if the carbon−carbon skeleton through the alkyl chains and the triple bond were oriented parallel to the plane of the HOPG surface. The predicted angle of the alkyl chain to the C−C triple bond of 146° compares well with the measured angle of 147° in the STM image. Furthermore, the offset between the two alkyl chains is predicted to be 1.43 Å, and the experimentally measured offset is 1.46 ± 0.05 Å.

Finally, a nitrile was observed in the STM image of 1-hydroxy-12-dodecanenitrile, $HO(CH_2)_{12}C{\equiv}N$ (Figure 19). The average length of the molecules is 18.3 ± 0.3 Å, which compares well with the expected length of 18.2 Å obtained from molecular modeling of the all-*trans*-conformation of the molecule. Both ends of the molecule are dark, leading to the conclusion that the nitrile is dark relative to the methylenes at both positive and negative bias. The OH groups are identifiable as the troughs of length 4.0 ± 0.1 Å and depth 0.91 ± 0.05 Å under negative bias, and of length 3.9 ± 0.1 Å and depth 0.60 ± 0.05 Å under positive bias. In either bias, the nitrile functionality is readily identified by its different length relative to the OH functionality. The topographic features of the nitrile and other functionalities are summarized in Table 4.

TABLE 4

molecule	bias	functional group features: length (Å)	functional group features: height (Å)
$C_{16}H_{33}HC{=}CHC_{17}H_{35}$	(+)	8.3 ± 0.1	0.48 ± 0.05
$C_{16}H_{33}HC{=}CHC_{17}H_{35}$	(−)	8.4 ± 0.1	0.56 ± 0.05
$H_3C(CH_2)_7C{\equiv}C(CH_2)_6OH$	(+)	4.3 ± 0.1	0.60 ± 0.05
$H_3C(CH_2)_7C{\equiv}C(CH_2)_6OH$	(−)	3.5 ± 0.1	0.45 ± 0.05
$HO(CH_2)_{12}C{\equiv}N$	(+)	3.3 ± 0.1	−0.36 ± 0.05
$HO(CH_2)_{12}C{\equiv}N$	(−)	3.7 ± 0.1	−0.91 ± 0.05

IV. Discussion

1. Reproducibility of the Images and Assignment of the Peaks to Features of the Molecular Overlayer. Prior workers have noted the difficulty in associating the features of an individual, selected STM image with those of a specific molecule deposited onto a surface.[2f−h,3,5] For instance, images of DNA on graphite have been questioned because of their lack of reproducibility as well as the fact that isolated regions of graphite (presumably near step edges and/or faults) have been observed to produce similar images under certain conditions.[4] In addition, Moiré patterns that produce periodic structures in STM images have been reported for simple, uncoated graphite surfaces under certain tip/sample bias conditions.[24,25] Before interpretation of the data obtained herein, we therefore must first address the issue of whether the data can reliably be associated with the molecules of concern.

Several aspects of the present system lend confidence to the assignment of the features in the images to the molecules of interest. First, since the sample preparation methods yielded well-packed monolayers of the desired molecules (as confirmed by several independent physical methods),[7−11,21] the STM images depicted in this study are not isolated, selected photographs that were observed only in one spot of one sample, but instead are characteristic of the images that can be obtained on any representative region of the graphite/alkane assembly.

A second feature that lends confidence to the association of these images with the molecular properties of interest is the systematic variation of the images in response to variation in the nature of the functional groups in the molecular overlayer. Over a dozen different functionalities were introduced into the molecules investigated in this work, and in each case these changes produced distinctive features in the STM images. The functionalities were positioned at the ends or centers or in nonsymmetric positions of the alkane chains, and the images of each system reflected the positions of the functional groups to within the experimental error of the measurement. Also, the lengths of the lamellae in the STM data assigned to the molecules in the overlayer changed in accord with the changes in the chemical composition of the overlayer, and the unit cell dimensions of the overlayer determined from the STM data agreed closely with those determined from low-angle X-ray diffraction measurements.[21] This type of systematic study not only lends confidence to the association of the image features to the molecules of interest but also allows a reliable comparison between the STM behavior of the various functional groups relative to the behavior of the methylene units in the alkane overlayers.

A third issue of possible concern is whether the data arose from some type of Moiré pattern, and instead of reflecting the molecular features in the overlayer actually are associated with the atomic positions of the graphite lattice. The distances and angles of the spots observed in the various high-resolution images of alkanes and alkanols do not all correspond to an integral graphite lattice spacing, but do closely correspond to the expected bond distances and bond angles for hydrocarbon

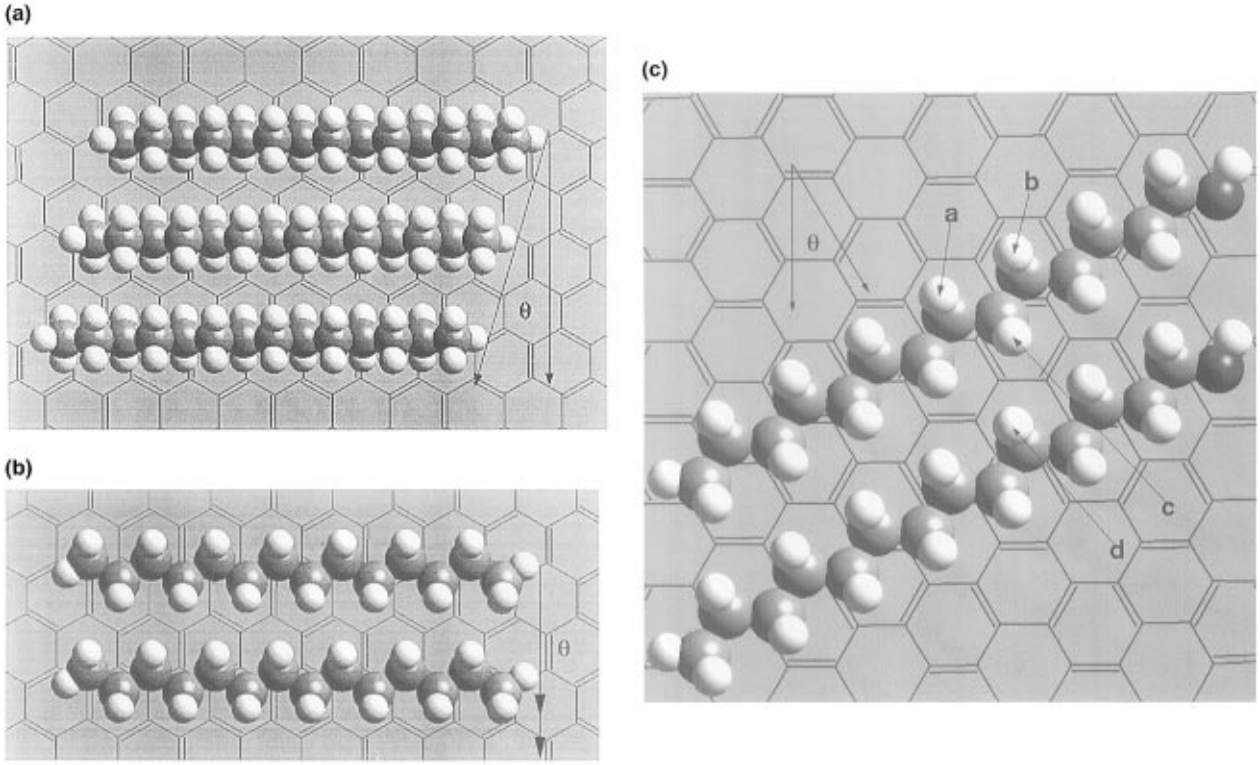

Figure 20. Schematic diagram of sterically favored packing arrangements of alkane and alkanol overlayers on graphite. (a) Alkanes oriented with their carbon−carbon skeletons perpendicular to the plane of the graphite surface. Structurally equivalent methylene units are offset in adjacent molecules and produce $\theta = 16°$ for an offset of 1.28 Å and an intermolecular spacing of 4.5 Å. (b) Alkanes oriented with their carbon−carbon skeletons parallel to the plane of the graphite surface. To minimize repulsions between methylene groups, adjacent molecules are expected to be in translational registry, with $\theta = 0°$, as shown. (c) Alkanols oriented with their carbon−carbon skeletons parallel to the graphite surface plane. An angle $\theta = 26°$ is produced in this packing arrangement, with the packing angle presumably driven by hydrogen-bonding interactions of the terminal OH groups (whose orientation and individual packing is only indicated schematically and cannot be assigned from the STM data available at present).

chains. Thus, for all of the reasons given above, we feel confident that the imaged features represent modulations in the tip/sample tunneling probability that are associated with the specific properties of the molecular overlayers under investigation.

2. Topography and Orientation of the Alkane and Alkanol Overlayers on Graphite Surfaces. The topography of the overlayer needs to be defined and identified so that the influence of electronic and topographic factors on the STM images can be evaluated individually. Prior studies of alkane overlayers on graphite have led to controversy because the STM images have been variously assigned either to reflect the positions of the carbon atoms in the graphite substrate or to reflect the positions of the atoms in the molecular overlayers.[12−20,25] The available experimental data do not allow reliable differentiation between these two possibilities, due to the similarity of the distances between adjacent carbons in a graphite STM image (2.46 Å) relative to the distances between adjacent hydrogen atoms in a *trans*-alkane chain (2.52 Å between adjacent methylene hydrogens and 2.56 Å between next-nearest methylene hydrogens).[24] If the STM images reflect the properties of the alkane overlayer, extended Hückel calculations have suggested that the hydrogen atoms on the methylene chains should dominate the observed STM spot pattern.[25] The STM data presented herein clearly indicate that the bright spots in the STM images of such systems are dominated by the features of the molecular overlayer and that the positions of the methylene hydrogens dominate the experimental images. These observations are in accord with the prior assignment of bright STM spots in the alkyl chain region of liquid crystals on graphite to the positions of the hydrogen atoms in the methylene chain portion of the molecules.[2b] The data presented herein also indicate that the alkanes and alkanols imaged at high resolution had their carbon−carbon skeletons oriented parallel to the graphite surface plane.

The orientations deduced from the high-resolution STM data are also supported by the molecular packing arrangements evident in the lower resolution STM images, i.e., those in Figure 1a−d. The most sterically favored packing for alkanes having their carbon−carbon skeleton oriented perpendicular to the graphite surface is obtained with the hydrogen atoms on adjacent alkane chains staggered by one-half of the distance between hydrogen atoms on next-nearest methylene units in the alkane chain (Figure 20a), i.e., by approximately 1.28 Å. With an intermolecular spacing of 4.5 Å, this type of packing would produce a value of the angle θ in Figure 20 of 16°. In contrast, the STM data of Figure 1d reveal that $\theta = 0°$ for $C_{35}H_{72}$ overlayers on graphite. This value of θ is consistent with the carbon−carbon skeleton of $C_{35}H_{72}$ being oriented parallel to the graphite surface plane, because a sterically favored packing in this molecular orientation exhibits registry perpendicular to the molecular axis between methylene units that are structurally equivalent but are located on adjacent alkane chains (Figure 20b). Thus, the packing arrangements observed for the alkanes in the lower resolution STM images support the orientational assignments deduced from the higher resolution STM images of Figure 3.

For alkanes absorbed on graphite, a rapid reorientation process has been proposed in which the carbon−carbon skeletons in an entire domain can change from being oriented parallel to the graphite surface plane to being oriented perpendicular to the graphite surface plane in the time elapsed between single STM image scans (but apparently the reorientation process has not been observed during the collection of an individual STM image).[25] As discussed above, such a process would require a sterically unfavorable packing arrangement, with significant

methylene−methylene repulsions between adjacent alkane chains, if a lamellar packing angle of $\theta \approx 0°$ were present in both orientations. We have only observed $\theta \approx 0°$ and have only observed high-resolution STM spot patterns that are consistent with a parallel orientation of the carbon−carbon skeleton with respect to the graphite surface for the alkane overlayers imaged during the course of this study. The predominant form of these alkane overlayers, as well as of the alkanol overlayers, therefore appears to be the one in which the carbon−carbon skeleton lies parallel to the graphite surface plane.[34]

It was also possible to identify the orientation of most of the other molecules imaged in our studies. A value of $\theta \approx 24-26°$ was observed for the molecular packing of alkanols and of substituted alkanols (Figures 1a-c, 4a, 5a, 10, 11, 13, 19). Note that although prior work has suggested that $C_{30}H_{61}OH$ lamellae on graphite are aligned parallel to the graphite lattice planes, due to observation of a lamellar packing angle, θ, of approximately 30°,[20] measurements of θ from the STM data of $C_{10}-C_{14}$ alkanols examined in this work and from low-angle X-ray diffraction data on related systems[21] show that $\theta = 24-26°$. This smaller angle indicates that the lamellae of these alkanol overlayers are not aligned with the underlying graphite lattice planes. On the basis of the steric packing arguments presented above, this angle indicates that the carbon−carbon skeleton of these molecules lies in a plane parallel to the graphite surface plane. In support of this conclusion, all of the substituted alcohols, except for the fluorinated species, $CF_3(CF_2)_3(CH_2)_{10}OH$ and $CF_3(CH_2)_{11}OH$, produced sufficiently high-resolution STM images such that the characteristic spot pattern displayed by the alkanols, indicating an orientation of the carbon−carbon skeleton parallel to the graphite surface plane, could be observed. In addition, the alkyne 7-hexadecyn-1-ol clearly has its carbon−carbon skeleton oriented parallel to the graphite surface plane, because a kink is observed between the molecular segments that lie on opposite sides of the carbon−carbon triple bond (Figure 18a). This observation further verifies the orientational assignments deduced from the high-resolution STM spot patterns of the other functionalized alkanols. These packing preferences indicate that the hydrogen-bonding interactions between the terminal OH groups dominate the intermolecular interactions of alkanol overlayers and induce a strong preference for the carbon−carbon skeleton of alkanols to be oriented parallel to the graphite surface plane.

3. Judging the Relative Importance of Topographic and Electronic Factors in Determining the STM Image Contrast of Functional Groups in Alkane/Alkanol Overlayers. The detailed analysis of the lengths, angles, and vertical contrast features of high-resolution STM images of a variety of molecular overlayers presented herein has allowed assignment of the locations of various functional groups relative to the "reference" methylene or OH units in such systems. Although a prior analysis, based on lower resolution STM images of $C_{30}H_{61}OH$ on graphite, has concluded that OH groups cannot be distinguished from the methylene regions of alkanol overlayers,[20] the data of Figures 1, 2, 4, 5, and 6 clearly show that the position of the OH group can be accurately located from the STM images of such systems. In addition, alkyl bromide, alkyl iodide, trifluoromethyl, and most of the other groups investigated in this study could be clearly distinguished both from the methylene units in the alkyl chain and from terminal OH groups. In fact, for the 12 functional groups investigated in this work, only Cl and OH functionalities were too similar to resolve from each other (i.e., were too similar to assign their relative locations if they were incorporated concurrently into an alkane/alkanol overlayer).

Given the ability to locate the apparent positions of the various functional groups, it is of interest to evaluate the factors that control their relative vertical image contrast. A recent theoretical study has concluded that the orbital mixing of insulating compounds into the energy levels of the substrate is responsible for producing the STM images of insulating overlayers.[25] The experimental data presented herein support this interpretation, but the data also underscore the significant variations in STM image contrast that can occur for different functional groups present in the molecular overlayer. One study has recently suggested that the STM tunneling contrast of halides in alkyl halide monolayers on graphite surfaces might be related to the atomic polarizability of the halide group.[20b] This hypothesis is not consistent with the functional group contrast observed in this work in which the polarizable OH, bromide, and chloride functionalities are dark relative to the methylene chains of alkanols but the iodide group is bright relative to these same methylene chain units.[35] As discussed in more detail below, the relationship between STM contrast and atomic polarizability also does not readily provide insight into the observed bias dependence of various functional groups in the STM images.

The data of Figures 1−19 imply that both topographic and electronic coupling factors are important in determining the STM image contrast. Clearly, since the images of the methylene units were dominated by the positions of the H atoms in the alkyl chain (Figures 2, 3), topography plays a dominant role in defining the image contrast of these regions of the molecular features. However, topography alone is not sufficient to explain the STM contrast of the functional groups. For example, based on topography alone, the CF_3 groups in the molecules $CF_3(CF_2)_3(CH_2)_{10}OH$ and $CF_3(CH_2)_{11}OH$ should appear bright, because the C−F bonds are longer than the C−H bonds in the parent alkanes and thus produce a functionality that projects topographically closer to the tip than does the unsubstituted methyl group. However, the tunneling probability over these functional groups must be low relative to the methylene groups since they appear dark in the STM image. Additionally, on the basis of size alone, the amine functionality should be dark since it is small relative to a methylene group, but it appears bright in the STM image.

We assign these differences to variations in the local electronic coupling of the various functional groups between the STM tip and sample relative to the electronic tip−sample coupling over the methylene units in the alkane section of these overlayers. Unfortunately, since all graphite and graphite-coated samples under ambient pressure conditions reported to date display an anomalously weak dependence of the tunneling current as the tip is retracted from the substrate, a quantitative interpretation of the STM image contrast mechanism of these samples is not possible at the present time. Despite this complication, it is possible to develop a qualitatively useful formalism for understanding the image contrast features that have been revealed during the present study. Using a McConnell superexchange formalism,[36] the electronic coupling between the tip and sample should increase as either the HOMO energy or LUMO energy of the substituted alkane approaches the Fermi level of the graphite substrate. At sufficiently large electronic coupling values, the functional group image should become bright in its STM contrast even if topographic effects alone would cause the tip to approach the sample.

A simple method for estimating the electronic coupling, and thus for predicting the image contrast of a given functional group in the STM images presented herein, would involve consideration of the ionization potentials of the various molecules of interest. When the coupling is dominated by the HOMO, functional groups with lower ionization potentials (IPs) than the corresponding alkane should appear bright in the STM image, while functional groups with higher ionization potentials

TABLE 5

molecule	ionization potential (eV)[32]
n-$(C_3H_7)_2NH$	7.8
Bu−S−S−Bu	8.5
$H_3C-S-CH_3$	8.7
$H_3CCH{=}CHCH_3$	9.1
n-C_4H_9I	9.2
$H_3CC{\equiv}CCH_3$	9.9
n-C_4H_9Br	10.2
n-C_4H_{10}	10.6
n-C_4H_9Cl	10.7
n-C_3H_7F	11.3
n-$C_3H_7C{\equiv}N$	11.7

should appear dark. Not only do the IP values affect the energy denominator in the expression for the electronic coupling term but lower IP values generally correlate with more a diffuse orbital structure of the functional groups of concern, which will enhance the wave function overlap term between the tip and the sample and thereby increase the value of the numerator in the electronic coupling expression.

This HOMO−IP model correlates remarkably well with the STM image contrast behavior observed in this work. Table 5 lists the ionization potentials of various substituted alkanes and related molecules of interest. In this framework, the disulfide and sulfide functionalities are predicted to exhibit a larger electronic coupling term than the methylene groups, and this expectation is in agreement with the observed STM images (Figures 14 and 15). The IP−STM contrast correlation predicts that if topographic effects are not predominant, an amine should be bright because of a large HOMO-derived electronic coupling term. This prediction is also in accord with the experimental STM data obtained in this work for dioctadecylamine, $(C_{18}H_{37})_2$-NH (Figure 16). Similar correlations are apparent between the image contrast and the ionization potentials for the alkyl chlorides, alkyl iodides, and fluoroalkyl functionalities studied in this work (Table 5 and Figures 8, 9, 11, and 12).

On the basis of the electronic coupling term estimated from the ionization potential of *trans*-2-butene (Table 5), a carbon−carbon double bond is expected to be bright, and the STM image of 17-pentatriacontene shows this to be the case at both positive and negative bias (Figure 17). A carbon−carbon triple bond should also appear bright, and this prediction is in accord with the STM data of 7-hexadecyn-1-ol overlayers (Figure 18). The ionization potential of a nitrile, however, is so large that its HOMO should be further from the Fermi level of the graphite than the HOMO of the corresponding alkane. Thus, as long as topography does not overwhelm the electronic coupling effect, the nitrile should be dark in STM image contrast despite the presence of a π orbital system. This prediction is consistent with the observed behavior of the nitrile functionality in the STM image of 1-hydroxy-12-dodecanenitrile (Figure 19).[37]

The alkyl bromide appears to be an exception to the predictions of the HOMO−IP electronic coupling model. The alkyl bromide is slightly larger than, and also has a slightly lower ionization potential than, the corresponding unsubstituted alkane. Nevertheless, the alkyl bromide functionality appears dark in the STM images (Figure 10). Detailed electronic structure calculations, described in the accompanying article, indicate a prominent role for the unoccupied orbitals of the alkane and alkyl bromide in dominating the electronic coupling between the tip and the sample. This more detailed model differs from the HOMO−IP approach in that it places more weight on specific electronic coupling effects that can arise from the contribution of the very energetic, but highly diffuse, LUMOs of the various substituted alkanes to the highly specific tunneling matrix element that is directed along the direction defined by the tip−sample gap. Since this direction is most heavily probed in the STM experiment, the orbital diffuseness becomes much more important in defining the overall electronic coupling matrix element in the STM image than it is in an intramolecular electron transfer experiment between a donor at one end of an alkyl chain and an acceptor at the other end of an alkyl chain. Further evidence for such differences are evident from the dominance of the carbon−carbon σ-bonding framework in determining electronic couplings in intramolecular electron transfer reactions relative to the dominance of the C−H bond positions in the STM images of alkanes. Thus, although the HOMO−IP approach seems to work remarkably well in predicting most of the STM image contrast behavior observed to date, the exact weighting of the HOMO and LUMO contributions to the tunneling matrix element in the general STM experiment will require additional elucidation both experimentally and theoretically.

4. Metrics of Various Functional Groups in STM Images. Although some functional groups produced STM features with dimensions that were in good accord with those expected from molecular modeling, other functional groups, such as amines and, most notably, disulfides, appeared to be much wider than might be expected. These large apparent length metrics cannot be consistently attributed solely to a lack of resolution in the STM data, since other portions of these images showed features that indicated significantly higher spatial resolution during the experiment.

At least three factors can contribute to this effect. First, the presence of a functional group can influence the local electronic coupling at neighboring methylene atoms in the substituted alkane, thereby creating the observed increased region of apparent functional group influence in the STM image. Another contributing factor is that the local molecular topography of the overlayer is often distorted around the functional group, resulting in a modification of the STM image over such distorted structural features. A semiquantitative estimate of these electronic and topographic effects has been obtained from *ab initio* electronic structure calculations that are described in the accompanying article. These calculations yield remarkably close agreement between the computed and observed STM images for most of the molecules investigated herein. Finally, an additional factor to be considered is that the observed current profile is actually the result of a two-dimensional problem, in which the tip−sample current is free to traverse any spatial path that provides the best electronic coupling between the tip and the sample at a given position in the scan. The dominant pathway when the tip is adjacent to, but not directly over, a functional group with a high electronic coupling term might involve through-space interactions to the functional group (in a direction predominantly parallel to the surface plane) as opposed to the more spatially direct but poorer electronic coupling path directly through the functional group and normal to the surface. This effect may play a role under the ambient pressure conditions under which the current study has been performed, since it is well-documented that the tip−sample tunneling current under such conditions shows an anomalously small distance decay exponent.[38] Without still higher resolution images, and perhaps low temperatures to freeze out any molecular motion and to eliminate the anomalous distance dependence of the tunneling current, we are unable to evaluate the relative importance of this factor in a quantitative fashion.

5. Symmetry Properties of the STM Image Contrast of Molecular Overlayers on Graphite. In addition to the theoretical expectations discussed above that address the relative contributions of topographic and electronic effects in determining the STM image contrast, it is also of interest to understand the dependence of the STM images on the tip/sample bias

voltage. A striking feature of the data for all functional groups investigated herein is the insensitivity of the image contrast to the tip/sample voltage polarity.[39] The density of states in the graphite substrate is nearly independent of polarity at low bias voltages.[40] However, the molecular overlayer is not expected, in general, to possess a symmetrical distribution with respect to the Fermi level of the graphite of the energy levels or of the individual tip/sample electronic coupling matrix elements of the system. Despite this expected asymmetry, the functional group contrast observed in the images of these overlayers (cf. Figures 1−19) was independent of the bias polarity. It is commonly assumed that tunneling into the surface should reflect the electronic coupling contours of the LUMO of the adsorbate and tunneling out of the surface should reflect the contours of the HOMO of the adsorbate.[2g,19] In this scenario, an asymmetry of the image contrast should generally be expected for functional groups having different locations of their HOMO and LUMO energies relative to the Fermi level of the substrate. We note, however, that this assumption strongly depends on the actual form of the potential distribution between the tip and the sample. We treat the general case below and then discuss the limiting situations as they apply to our experimental data in order to develop a fundamental understanding of the observed symmetry in image contrast with respect to bias polarity.

At a given bias voltage and location over the substrate, the tunneling current is a function of the density and occupancy of the electronic states in the tip, the density and occupancy of the electronic states in the substrate, and the quantum mechanical matrix elements that couple the electronic states in tip and substrate. One expression that can be used to evaluate the STM current, based on the Fermi golden rule approach to the calculation of the electronic coupling between an electron donor and an electron acceptor, is[41]

$$i = \frac{2\pi e}{\hbar}\int\int d^3\mathbf{k}_m d^3\mathbf{k}_t |H_{mt}(\mathbf{k}_m,\mathbf{k}_t)|^2[f(\epsilon_t) - f(\epsilon_m)] \times \delta(\epsilon_t - \epsilon_m - e\upsilon) \quad (1)$$

In this equation, the **k**'s refer to the orbitals in the substrate (M) and in the tip (T), and H_{mt} represents the electronic coupling matrix elements between these states at each energy and at each point in space. The occupancies of the orbitals at an energy ϵ (measured in excess of the respective Fermi levels of the tip and the substrate) are given by $f(\epsilon_t)$ and $f(\epsilon_m)$ (the Fermi−Dirac distribution functions $[1 + \exp(\epsilon/k_BT)]^{-1}$ in the tip and substrate, respectively). The delta function in the expression of eq 1 ensures that tunneling occurs only between states of the same energy in the tip and the substrate and also accounts for the relative energy difference between the tip and substrate that is induced by applying a bias voltage, υ, across the tip−sample gap. The bias voltage can be expressed as $\upsilon = \phi_t - \phi_m - (\phi_t^e - \phi_m^e)$, where the ϕ's denote electrostatic potentials and the e superscript denotes the value at zero current.

For a vacuum gap, the matrix elements H_{mt} are given by the well-known quantum mechanical expression for electron tunneling through a vacuum.[42] For the passage of the current across an adsorbed monolayer B, the matrix elements H_{mt} must instead describe the tip/sample coupling that arises from the presence of the orbitals in the molecular overlayer. In a superexchange formalism to calculate this coupling, H_{mt} can be expressed as[43]

$$H_{mt}(\mathbf{k}_m,\mathbf{k}_t) = \sum_\beta H_{m\beta}H_{\beta t}/(E_m - E_\beta) \quad (2)$$

where $H_{m\beta}(\mathbf{k}_m)$ denotes the matrix element coupling orbital $\mathbf{k}_m$ in M to an orbital β of the molecular overlayer and $H_{\beta t}(\mathbf{k}_t)$ denotes the matrix element coupling β to the orbital $\mathbf{k}_t$ in T. The energy denominator is given by $E_m - E_\beta$, where E_m and E_β are the energies of the orbitals in M and B, with $E_m = \bar{\mu}_m + \epsilon_m$, $\bar{\mu}_m$ being the electrochemical potential (Fermi level) of M, $\bar{\mu}_m = \mu_m^0 - e\phi_m$. (Similarly, below, $\bar{\mu}_t = \mu_t^0 - e\phi_t$ and we note that the delta function constraint in eq 1 can be shown to be equivalent to $\bar{\mu}_m + \epsilon_m = \mu_t + \epsilon_t$.) The expression of eq 2 thus arises from a simple perturbation theory approach to evaluating the electronic coupling between the tip and substrate states due to the presence of the orbitals of the intervening overlayer.

Of primary concern is the symmetry of i with respect to the value of the tip−substrate bias, υ. When the bias is changed, the relation of the M and T energy levels is changed. This effect is manifested in eq 1 through the constraint imposed by the delta function, which ensures an isoenergetic tunneling of electrons through the tip−substrate gap. In addition, the energy denominator $E_m - E_\beta$ in eq 2, which determines the electronic coupling terms H_{mt} at a given tip−sample bias voltage, is a function of bias voltage. Following the recent work of Marcus,[43] the mean potential of the bridge levels β can be approximated to be $^1/_2(\phi_m + \phi_t)$. In other words, the molecular overlayer experiences a potential drop that is ∼1/2 of the total potential dropped between the tip and the substrate. In this case one can show that[43]

$$E_m - E_\beta = \frac{1}{2}(\mu_m^0 + \mu_t^0 + \epsilon_m + \epsilon_t) - E_\beta^0 \quad (3)$$

where E_β^0 is the value of E_β at zero potential.

Use of eq 3 to address quantitatively the bias dependence of the image contrast implies replacement of υ with $-\upsilon$ in eq 1. A change in sign of υ to $-\upsilon$ is equivalent to interchanging ϵ_m and ϵ_t according to the delta function in eq 1. This interchange changes the sign of the term in square brackets in eq 1, but clearly (eq 3) leaves $E_m - E_\beta$ unaffected. Thus, we have

$$i(\upsilon) = -i(-\upsilon) \quad (4)$$

if $H_{m\beta}H_{\beta t}$ is independent of, or only weakly dependent on, υ.

On the basis of the discussion above, in the regime of linear $I-V$ behavior wherein the molecule experiences an equivalent potential drop regardless of whether the tip or the sample is biased away from equilibrium, the electronic coupling is the sum of the coupling matrix elements through the HOMO and LUMO, regardless of the bias condition. This summation over all available coupling orbitals necessarily produces a symmetry with respect to bias and provides a natural explanation for the observation of symmetry in image contrast that was observed experimentally for all systems studied.

An alternative possibility is that the adsorbate is in strong electrical contact with the sample and that the applied bias predominantly affects the potential across the adsorbate/tip region but not between the sample and the adsorbate. In this case, a large enough bias perturbation would produce a differential electronic coupling to the LUMO with the tip negative of the Fermi level and to the HOMO with the tip biased positive relative to the Fermi level of the substrate. This situation would, however, require a fortuitously symmetric (or nearly so) positioning of the HOMO and LUMO levels relative to the Fermi level of the graphite substrate and would also require nearly equal orbital diffuseness in the HOMO and LUMO for all of the functional groups investigated in this study. As described in the accompanying article, theoretical calculations do not support the occurence of this unlikely set of coincidences for any of the molecules studied in this work. Variation of the Fermi level of the substrate over a sufficiently wide range of energy while maintaining all of the other desirable properties of the graphite/alkane−alkanol overlayer system

would thus be of interest to probe this effect further. Such experiments might be possible through the use of substrates such as H-terminated Si or TaS_2, and such systems are being investigated experimentally at present.

V. Conclusions

We have shown that it is possible to distinguish between the topographic locations of various functional groups on the basis of their image contrast and apparent geometric properties using STM data obtained at room temperature and atmospheric pressure. Such studies are made possible by the investigation of ordered overlayers of molecular systems, which can be reproducibly imaged and varied chemically in a systematic fashion. An analysis of high-resolution STM images of alkanes and alkanols reveals that topographic factors dominate the image contrast of such systems and also indicates that the molecules in these overlayers are oriented with their carbon−carbon skeleton parallel to the graphite surface. Additionally, the bright spots in these molecular images are predominantly determined by the positions of the hydrogen atoms on the methylene units of the alkyl chains. The STM contrast of the various functional groups investigated in this work not only was a function of topography but also was influenced by the local electronic coupling. For molecules in which electronic effects overwhelmed topographic effects in dominating the image contrast, electronic coupling between both the HOMO and LUMO must be considered at low and moderate bias in an STM image, leading to an explanation of the observed functional group image contrast as well as an explanation of the bias symmetry of several representative functional groups.

Acknowledgment. We acknowledge the NSF, grants CHE-9634152 (N.S.L.), CHE-9522179 (W.A.G.), CHE-9610164 (H.B.G.), and ASC-9217368 (W.A.G.), for partial support of this work. C.C. acknowledges the NIH for a training grant, and we also acknowledge helpful discussions with Dr. J. Miller of Argonne National Laboratory regarding orbital coupling issues.

References and Notes

(1) Binnig, G.; Rohrer, H. *Angew. Chem.* **1987**, *99*, 622; *Angew. Chem., Int. Ed. Engl.* **1987**, *26*, 606.

(2) For STM of organic materials, see: (a) Frommer, J. *Angew. Chem., Int. Ed. Engl.* **1992**, *31*, 1298. (b) Smith, D.; Hörber, J.; Binnig, G.; Nejoh, H. *Nature* **1990**, *344*, 641. Foster, J.; Frommer, J. *Nature* **1988**, *333*, 542. (c) Smith, D.; Hörber, J.; Gerber, C.; Binnig, G. *Science* **1989**, *245*, 43. (d) Ludwig, C.; Gompf, B.; Glatz, W.; Petersen, J.; Eisenmenger, W. *Z. Phys. B.* **1992**, *86*, 397. (e) Smith, D.; Heckl, W. *Nature* **1990**, *346* 616. (f) Ohtani, H.; Wilson, R.; Chiang, S.; Mate, C. *Phys. Rev. Lett.* **1988**, *60*, 2398. (g) Lippel, P.; Wilson, R.; Miller, M.; Wöll, C.; Chiang, S. *Phys. Rev. Lett.* **1989**, *62*, 171. (h) Hallmark, V.; Chiang, S.; Brown, J.; Wöll, C. *Phys. Rev. Lett.* **1991**, *66*, 48. (i) Kim, Y.; Bard, A. *Langmuir* **1992**, *8*, 1096. (j) Smith, D.; Bryant, A.; Quate, C.; Rabe, J.; Gerber, C.; Swalen, J. *Proc. Natl. Acad. Sci. U.S.A.* **1987**, *84*, 969. (k) McMaster, T.; Carr, H.; Miles, M.; Cairns, P.; Morris, V. *Macromolecules* **1991**, *24*, 1428. (l) Yang, R.; Naoi, K.; Evans, D.; Smyrl, W.; Hendrickson, W. *Langmuir* **1991**, *7*, 556. (m) Wilson, R.; Meijer, G.; Bethune, D.; Johnson, R.; Chambliss, D.; de Vries, M.; Hunziker, H.; Wendt, H. *Nature* **1990**, *348*, 621. (n) Li, Y.; Chander, M.; Patrin, J.; Weaver, J.; Chibante, L.; Smalley, R. *Science* **1991**, *253*, 429. (o) Allen, M.; Ballooch, M.; Subbiah, S.; Tench, R.; Siekhaus, W.; Balhorn, R. *Scanning Microsc.* **1991**, *5*, 625. (p) Youngquist, M.; Driscoll, R.; Coley, T.; Goddard, W.; Baldeschwieler, J. *J. Vac. Sci. Technol. B* **1991**, *9*, 1304. (q) Lu, X.; Hipps, K. W.; Wang, X. D.; Mazur, U. *J. Am. Chem. Soc.* **1996**, *118*, 7197.

(3) For example, see: Driscoll, R. J.; Youngquist, M. G.; Baldeschwieler, J. D. *Nature* **1990**, *346*, 294.

(4) (a) Clemmer, C.; Beebe, T. *Science* **1991**, *251*, 640. (b) Chang, H.; Bard, A. *Langmuir* **1991**, *7*, 1143.

(5) Kim, Y.; Long, E. C.; Barton, J. K.; Lieber, C. M. *Langmuir* **1992**, *8*, 496.

(6) (a) Patrick, D. L.; Cee, V. J.; Beebe, T. *Science* **1994**, *265*, 231. (b) Patrick, D. L.; Cee, V. J.; Beebe, T. P. *J. Phys. Chem.* **1996**, *100*, 8478.

(7) Groszek, A. J. *Nature* **1962**, *196*, 531.

(8) Findenegg, G. H.; Lippard, M. *Carbon* **1987**, *25*, 119.

(9) Parfitt, G. D.; Willis, E. *J. Phys. Chem.* **1964**, *68*, 1780.

(10) Groszek, A. J. *Proc. R. Soc. London Ser. A* **1970**, *314*, 473.

(11) Findenegg, G. H *J. Chem. Soc., Faraday Trans.* **1973**, *69*, 1069.

(12) Rabe, J. P.; Buchholz, S. *Science* **1991**, *253*, 424.

(13) Cincotti, S.; Rabe, J. P. *Appl. Phys. Lett.* **1993**, *62*, 3531.

(14) McGonigal, G. C.; Bernhardt, R. H.; Thomson, D. J. *Appl. Phys. Lett.* **1990**, *57*, 28.

(15) McGonigal, G. C.; Bernhardt, R. H.; Yeo, Y.; Thomson, D. J. *J. Vac. Sci. Technol. B* **1991**, *9*, 401.

(16) Buchholz, S.; Rabe, J. P. *Angew. Chem., Int. Ed. Engl.* **1992**, *31*, 189.

(17) Yeo, Y. H.; McGonigal, G. C.; Thomson, D. J. *Langmuir* **1993**, *9*, 649.

(18) Buchholz, S.; Rabe, J. P. *J. Vac. Sci. Technol. B* **1991**, *2*, 1126.

(19) Rabe, J. P.; Buchholz, S.; Askadskaya, L. *Synth. Met.* **1993**, *54*, 349.

(20) (a) Venkataraman, B.; Flynn, G. W.; Wilbur, J. L.; Folkers, J. P.; Whitesides, G. M. *J. Phys. Chem.* **1995**, *99*, 8684. (b) Cyr, D. M.; Venkataraman, B.; Flynn, G. W.; Black, A.; Whitesides, G. M. *J. Phys. Chem.* **1996**, *100*, 13747. (c) Cyr, D. M.; Venkataraman, B.; Flynn, G. W. *Chem. Mater.* **1996**, *8*, 1600.

(21) Morishige, K.; Takami, Y.; Yokota, Y. *Phys. Rev. B* **1993**, *48*, 8277.

(22) (a) Larsson, U.; Carlson, R.; Leroy, J. *Acta Chem. Scand.* **1993**, *47*, 380. (b) Bennett, G. M.; Gudgeon, H. *J. Chem. Soc. (London)* **1938**, 1679.

(23) *CRC Handbook of Chemistry and Physics*; Weast, R. C., Lide, D. R., Astle, M. J., Beyer, W. H., Eds.; CRC Press: Boca Raton, 1989.

(24) Vollhardt, P. C. *Organic Chemistry*; W. H. Freeman: New York, 1987; pp 58−59.

(25) Liang, W.; Whangbo, M. H.; Wawkuschewski, A.; Cantow, H. J.; Magonov, S. N. *Adv. Mater.* **1993**, *5*, 817.

(26) Kuwabara, M.; Clarke, D. R.; Smith, D. A. *Appl. Phys. Lett.* **1990**, *56*, 2396.

(27) Xhie, J.; Sattler, K.; Ge, M.; Venkateswaran, N. *Phys. Rev. B* **1993**, *47*, 15835.

(28) Rabe, J. P.; Buchholz, S.; Askadskaya, L. *Synth. Met.* **1993**, *54*, 349.

(29) Wawkuschewski, A.; Cantow, H. J.; Magonov, S. N.; Möller, M.; Liang, W.; Whangbo, M. H. *Adv. Mater.* **1993**, *5*, 821.

(30) Pomerantz, M.; Aviram, A.; McCorkle, R. A.; Li, L.; Schrott, A. G. *Science* **1992**, *255*, 1115.

(31) Niki, K. Personal communication.

(32) Mizutani, W.; Shigeno, M.; Ono, M.; Kajimura, K. *Appl. Phys. Lett.* **1990**, *56*, 1974.

(33) Okumura, A.; Miuamura, K.; Gohshi, Y. *Jpn. J. Appl. Phys.* **1992**, *31*, 3452.

(34) We note that the image that was interpreted as evidence for the alkane reorientation process was obtained under conditions of significant thermal drift in order to produce the rectangular spot pattern for the methylene units in the alkyl chain. In addition, a recent neutron diffaction study has concluded that vapor-deposited $C_{32}D_{66}$ overlayers are adsorbed on graphite with their carbon−carbon skeletons oriented paralled to the graphite surface plane, in accord with our STM images: Herwig, K. W.; Matthies, B.; Taub, H. *Phys. Rev. Lett.* **1995**, *75*, 3154.

(35) Note that the image contrast observed in this work for alkanol and substituted alkanol overlayers on graphite is in good agreement with STM images reported recently for substituted alkane overlayers on graphite. This earlier study concluded that OH and Cl functionalities could not be observed by STM,[20] and thus these groups were ordered as similar in STM image contrast to the methyl and methylene functionalities of substituted alkane overlayers. This ordering seems to require modification in view of the STM data presented in this work. Data for an alkyl bromide ($C_{22}H_{45}Br$) overlayer indicated that the bromide group was typically dark in STM image contrast relative to the methylene chains of this overlayer,[20] in agreement with the STM data for overlayers of $Br(CH_2)_{12}OH$ displayed in Figure 10. When the $C_{22}H_{45}Br$ films were imaged continuously for a significant time period, the Br groups were reported to change contrast to bright.[20] Such changes in image contrast have not been observed in our work, presumably because the substituted alkanols used herein are more constrained in their orientational preferences than are the substituted alkanes. This difference is reasonable because of the presence of the hydrogen-bonding network between the OH groups in the alkanol overlayer. As described in more detail in the accompanying article, a change in STM contrast from dark to bright would be expected if the Br group were to move from a *trans*-position to a *gauche*-position relative to the carbon−carbon skeleton of an alkane chain. Such a process might explain the image contrast changes observed for the alkyl bromide after significant observation time under the STM tip.[20]

(36) McConnell, H. M. *J. Chem. Phys.* **1961**, *35*, 508.

(37) STM data for a nitrile group in an overlayer of the liquid crystal 4′-*n*-alkyl-4-biphenyl have been obtained previously.[2a−c,e,6a] Smith *et al.* reported that the nitrogen atom of the nitrile appeared to be brighter than the carbon atom of the nitrile.[2b] Inspection of the published images of the

liquid crystals appears to indicate that it would be extremely difficult to identify atomically localized regions of the nitrile group on the basis of the STM data available to date.

(38) (a) Binnig, G.; Rohrer, C.; Gerber, C.; Weibel, E. *Appl. Phys. Lett.* **1982**, *40*, 178. (b) Gimzewski, J. K.; Möller, R. *Phys. Rev. B* **1987**, *36*, 1284. (c) Gimzewski, J. K.; Möller, R.; Pohl, D. W.; Schlittler, R. R. *Surf. Sci.* **1987**, *189*, 15. (d) Mamin, H. J.; Ganz, E.; Abraham, D. W.; Thomson, R. E.; Clarke, J. *Phys. Rev. B* **1986**, *34*, 9015.

(39) Preliminary results of the STM images of stearone, $(C_{17}H_{35})_2CO$, indicate that this symmetry with bias may not always be observed. At negative sample bias, a bright feature associated with the carbonyl functionality is observed to have a length of 9.0 Å and height of 0.22 Å. At positive bias, however, a dark feature associated with the carbonyl functionality is observed to have a length of 8.5 Å and a depth of 0.25 Å. The STM image contrast of this molecule, and related ketones, is under further investigation in order to ascertain the origin of this effect.

(40) *Metals: Phonon States, Electron States and Fermi Surfaces*; Hellwege, K. H., Olsen, J. L., Eds.; Springer-Verlag: Berlin, 1981.

(41) Hui, O.-Y.; Kallebring, B.; Marcus, R. A. *J. Chem. Phys.* **1993**, *98*, 7565.

(42) Hansma, P. K.; Tersoff, J. *J. Appl. Phys*. **1987**, *61*, R21.

(43) Marcus, R. A. *J. Chem. Soc., Faraday Trans.* **1996**, *92*, 3905.